



Quantum fluctuations approach to the nonequilibrium GW approximation: Density correlations and dynamic structure factor

Erik Schroedter, Björn Jakob Wurst, Jan-Philip Joost , and Michael Bonitz *

*Institut für Theoretische Physik und Astrophysik, Christian-Albrechts-Universität zu Kiel, D-24098 Kiel, Germany
and Kiel Nano, Surface and Interface Science KiNSIS, Kiel University, Kiel, Germany*



(Received 31 May 2023; revised 22 September 2023; accepted 19 October 2023; published 6 November 2023)

The quantum dynamics of correlated fermionic or bosonic many-body systems following external excitation can be successfully studied using nonequilibrium Green functions (NEGFs) or reduced density matrix methods. Approximations are introduced via a proper choice of the many-particle self-energy or decoupling of the BBGKY-hierarchy, respectively. These approximations are based on Feynman's diagram approaches or on cluster expansions into single-particle and correlation operators. In a recent paper [E. Schroedter, J.-P. Joost, and M. Bonitz, *Condens. Matter Phys.* **25**, 23401 (2022)] we presented a different approach in which, instead of equations of motion for the many-particle NEGF (or density operators), equations for the correlation functions of fluctuations are analyzed. In particular, we derived the stochastic GW and polarization approximations that are closely related to the nonequilibrium GW approximation. Here, we extend this approach to the computation of two-time observables depending on the specific ordering of the underlying operators. In particular, we apply this extension to the calculation of the density correlation function and dynamic structure factor of correlated Hubbard clusters in and out of equilibrium.

DOI: [10.1103/PhysRevB.108.205109](https://doi.org/10.1103/PhysRevB.108.205109)

I. INTRODUCTION

The dynamics of quantum many-body systems following external excitation are of high interest in many areas, such as dense plasmas, nuclear matter, ultracold atoms, or correlated solids. There is a large variety of methods available to simulate such systems, which include real-time quantum Monte Carlo, density matrix renormalization group approaches, time-dependent density functional theory, and quantum kinetic theory. Among the many-particle observables that are accessible in experiments, a central role is played by the correlation functions of density or spin fluctuations and the corresponding dynamic structure factors; see, e.g., Ref. [1] for an overview. To compute these quantities with correlation effects taken into account, there exist a variety of equilibrium simulations. The most accurate results have been obtained from quantum Monte Carlo simulations for correlated solids (e.g., Refs. [2–4]), as well as warm dense matter [5–7] where also the nonlinear response has been analyzed [8–10]. In addition, there exist a variety of nonequilibrium approaches, including dynamical mean-field theory (e.g., Refs. [11,12]), time-dependent DMRG (e.g., Ref. [13]), and nonequilibrium Green functions (NEGFs) (cf. Ref. [14] and references therein).

Here we concentrate on the NEGF approach [15–17] because it can rigorously describe the quantum dynamics of correlated systems in more than one dimension; see, e.g., Ref. [18]. However, NEGF simulations are computationally expensive, primarily due to their cubic scaling with the sim-

ulation time N_t (number of time steps). Only recently could linear scaling with N_t be achieved within the G1-G2 scheme [19,20], which could be demonstrated even for advanced self-energies, including the GW and the T -matrix approximations. Even the nonequilibrium dynamically screened ladder approximation, which self-consistently combines dynamical screening and strong coupling, is now feasible, at least for lattice models [21,22].

The advantage of time linear scaling of the G1-G2 scheme comes at a price: the simultaneous propagation of the time-diagonal single-particle and correlated two-particle Green functions, $G_1(t)$ and $\mathcal{G}_2(t)$, requires a large computational effort for computing and storing all matrix elements of \mathcal{G}_2 . For example, the CPU time of GW -G1-G2 simulations scales as N_b^6 , where N_b is the basis dimension. Even though this difficulty can be relieved using massively parallel computer hardware or embedding self-energy approaches [16,23], it is well worth it to look for alternative formulations of the problem that are more suitable for computations, ideally without loss of accuracy.

In Ref. [24], an alternative formulation of the quantum many-body problem was presented that is based on a stochastic approach to the dynamics of quantum fluctuations. Extending earlier stochastic concepts in the kinetic theory of classical systems, due to Klimontovich (see, e.g., Refs. [25–27]), and quantum systems by Ayik, Lacroix [28–30], and many others (see, e.g., Refs. [31,32]), we derived an equation of motion for the single-particle fluctuations, $\delta\hat{G}$ [see Eq. (8) below], that is equivalent to the nonequilibrium GW approximation in the weak-coupling limit.

Here we extend the results of Ref. [24] to the nonequilibrium dynamics of two-time quantities (and their Fourier

*bonitz@theo-physik.uni-kiel.de

transform) such as the density correlation function (and the dynamic structure factor). This first requires us to obtain a semiclassical approach to the computation of commutators of operators. This is achieved within a multiple ensembles (MEs) approach. With this extension, we are then able to compute the density response function and dynamic structure factor, both in the ground state and for a far-from-equilibrium situation following an external excitation. This constitutes a significant extension of the quantum fluctuations approach of Ref. [24] that is applicable to large systems and long simulation times.

This paper is structured as follows. In Sec. II we introduce the quantum fluctuations approach and establish its connection to the exchange-correlation function of NEGF theory. Here we also derive the expressions for the dynamic structure factor and the density response function. This is followed, in Sec. III, by an introduction to our stochastic approach to quantum fluctuations. Then, in Sec. IV we present our numerical results for small- and moderate-sized Hubbard clusters. A summary and outlook are given in Sec. V.

II. QUANTUM FLUCTUATIONS APPROACH

A. Notation and definitions

In the following, we use the formalism of second quantization, which is characterized by the bosonic/fermionic creation (\hat{c}_i^\dagger) and annihilation (\hat{c}_i) operators and the respective single-particle basis of the underlying single-particle Hilbert space \mathcal{H} , which induces the so-called Fock space \mathcal{F} . These operators have the following properties:

$$[\hat{c}_i, \hat{c}_j^\dagger]_{\mp} = \delta_{ij}, \quad [\hat{c}_i, \hat{c}_j]_{\mp} = [\hat{c}_i^\dagger, \hat{c}_j^\dagger]_{\mp} = 0, \quad (1)$$

where the upper/lower sign refers to bosons/fermions, respectively. Here, we consider a quantum many-particle system, which is described by a generic Hamiltonian of the form

$$\hat{H}(t) = \sum_{ij} h_{ij}(t) \hat{c}_i^\dagger \hat{c}_j + \frac{1}{2} \sum_{ijkl} w_{ijkl}(t) \hat{c}_i^\dagger \hat{c}_j^\dagger \hat{c}_l \hat{c}_k, \quad (2)$$

where h denotes the single-particle contributions (from the kinetic energy and an external potential) and a general pair interaction w . Notice that both h and w are allowed to be time-dependent in order to account for changes in the external potential, e.g., due to lasers [33], particle impact [34–36], or a change of the confinement potential [18], whereas the time dependence of the interaction potential allows for the computation of a correlated initial state from an uncorrelated state via the adiabatic switching method. Additionally, the interaction tensor w obeys the symmetries

$$w_{ijkl}(t) = w_{jikl}(t) = [w_{klij}(t)]^*. \quad (3)$$

The central quantity of the NEGF theory is the one-body Green function, which is defined on the Keldysh contour \mathcal{C} for contour-time arguments z and z' as

$$G_{ij}(z, z') := \frac{1}{i\hbar} \langle \mathcal{T}_{\mathcal{C}} \{ \hat{c}_i(z) \hat{c}_j^\dagger(z') \} \rangle, \quad (4)$$

where $\mathcal{T}_{\mathcal{C}}$ denotes the time-ordering operator on the contour. Averaging is performed with the correlated unperturbed density operator of the system. In the following, it will be sufficient to consider the correlation functions G^{\gtrless} for real time

arguments. We define these functions and the corresponding operators as

$$G_{ij}^{\gtrless}(t, t') := \langle \hat{G}_{ij}^{\gtrless}(t, t') \rangle, \quad (5)$$

$$\hat{G}_{ij}^<(t, t') := \pm \frac{1}{i\hbar} \hat{c}_j^\dagger(t') \hat{c}_i(t), \quad (6)$$

$$\hat{G}_{ij}^>(t, t') := \frac{1}{i\hbar} \hat{c}_i(t) \hat{c}_j^\dagger(t'). \quad (7)$$

Additionally, we will only consider G^{\gtrless} on the time-diagonal ($t = t'$) and, therefore, denote $G^{\gtrless}(t) := G^{\gtrless}(t, t)$. On the real-time diagonal, the lesser component of the one-body Green function is proportional to the single-particle density matrix, $n_{ij}(t) := \langle \hat{c}_j^\dagger(t) \hat{c}_i(t) \rangle = \pm i\hbar G_{ij}^<(t)$. In this paper, we will not consider bosons in a condensate and thus no anomalous correlators will appear. However, an extension of our approach to that case is straightforward.

The cornerstone of the quantum fluctuations approach, as developed in Ref. [24], is the single-particle fluctuation operator,

$$\delta \hat{G}_{ij}(t) := \hat{G}_{ij}^<(t) - G_{ij}^<(t) \equiv \hat{G}_{ij}^>(t) - G_{ij}^>(t), \quad (8)$$

where it was used that, on the time-diagonal, $\hat{G}_{ij}^>(t) - \hat{G}_{ij}^<(t) = \frac{1}{i\hbar} \delta_{ij}$ for all t and, obviously, $\langle \delta \hat{G}_{ij}(t) \rangle = 0$. Next, we define general two-particle fluctuations and the associated correlation function as

$$\hat{L}_{ijkl}(t, t') := \delta \hat{G}_{ik}(t) \delta \hat{G}_{jl}(t'), \quad (9)$$

$$L_{ijkl}(t, t') := \langle \hat{L}_{ijkl}(t, t') \rangle, \quad (10)$$

$$L_{ijkl}(t) := L_{ijkl}(t, t). \quad (11)$$

The two-particle correlation function, Eq. (10), can be considered a special case of the exchange-correlation (XC) function in standard NEGF theory [16],

$$L_{ijkl}(z_1, z_2, z'_1, z'_2) := G_{ijkl}^{(2)}(z_1, z_2, z'_1, z'_2) - G_{ik}(z_1, z'_1) G_{jl}(z_2, z'_2), \quad (12)$$

where $G^{(2)}$ is the two-particle Green function defined on the Keldysh contour,

$$G_{ijkl}^{(2)}(z_1, z_2, z'_1, z'_2) := -\frac{1}{\hbar^2} \langle \mathcal{T}_{\mathcal{C}} \{ \hat{c}_i(z_1) \hat{c}_j(z_2) \hat{c}_l^\dagger(z'_2) \hat{c}_k^\dagger(z'_1) \} \rangle. \quad (13)$$

Depending on the index combinations, the function L , Eq. (10), is related to various correlation functions. In particular, for $i = k$ and $j = l$, it gives access to density fluctuations and the dynamic structure factor [37], whereas other combinations contain information about the current correlations.

B. Quantum dynamics in terms of fluctuations

The equation of motion (EOM) for $G^<$ on the time-diagonal can be given in terms of two-particle fluctuations L [38],

$$i\hbar \frac{d}{dt} G_{ij}^<(t) = [h^H, G^<]_{ij}(t) + [I + I^\dagger]_{ij}(t), \quad (14)$$

where we introduced an effective single-particle Hartree Hamiltonian,

$$h_{ij}^H(t) := h_{ij}(t) \pm i\hbar \sum_{kl} w_{ikjl}(t) G_{lk}^<(t), \quad (15)$$

and a collision term,

$$I_{ij}(t) := \pm i\hbar \sum_{klp} w_{iklp}(t) L_{plkj}(t). \quad (16)$$

We can equivalently write

$$[I + I^\dagger]_{ij}(t) = \langle [\delta\hat{U}^H, \delta\hat{G}]_{ij}(t) \rangle, \quad (17)$$

with the operator of an effective single-particle Hartree potential induced by fluctuations,

$$\delta\hat{U}_{ij}^H(t) := \pm i\hbar \sum_{kl} w_{ikjl}(t) \delta\hat{G}_{lk}(t). \quad (18)$$

Equation (16) can also be equivalently expressed in terms of symmetric two-particle fluctuations, i.e.,

$$I_{ij}(t) = S_{ij}(t) + I_{ij}^S(t), \quad (19)$$

with the symmetrized collision term given by

$$I_{ij}^S(t) := \pm \frac{i\hbar}{2} \sum_{klp} w_{iklp}(t) \{L_{plkj}(t) + L_{lpjk}(t)\} \quad (20)$$

and a symmetrization contribution of the form

$$S_{ij}(t) := \frac{1}{2} \sum_{kl} w_{kljk}(t) G_{il}^<(t). \quad (21)$$

The EOM for any quantity that depends on products of $\delta\hat{G}$, such as L , can simply be derived from the EOM for the single-particle fluctuation operator, which is given by

$$i\hbar \frac{d}{dt} \delta\hat{G}_{ij}(t) = [h^H, \delta\hat{G}]_{ij}(t) + [\delta\hat{U}^H, G^<]_{ij}(t) + [\delta\hat{U}^H, \delta\hat{G}]_{ij}(t) - \langle [\delta\hat{U}^H, \delta\hat{G}]_{ij}(t) \rangle. \quad (22)$$

Note that Eq. (22) is nonlinear in $\delta\hat{G}$, which leads, in the EOMs for L , to terms that are cubic in $\delta\hat{G}$ and thus a coupling to three-particle fluctuations. Therefore, we require approximations decoupling the fluctuations hierarchy.

C. Quantum polarization approximation

The approximation we want to consider here is the quantum analog of the classical polarization approximation, which is known to be equivalent to the Balescu-Lenard kinetic equation, which describes scattering of charged particles on a dynamically screened pair potential [27]. Additionally, the polarization approximation is the classical limit of the nonequilibrium GW approximation [39]. On the level of single-particle fluctuations, the quantum polarization approximation (PA) follows by assuming

$$\delta\hat{L}_{ijkl}(t) \approx \delta\hat{L}_{ijkl}^{(0)}(t), \quad (23)$$

where $\delta\hat{L}$ denotes fluctuations of two-particle fluctuations included in the last line of Eq. (22), and $\delta\hat{L}^{(0)}$ can be interpreted as fluctuations of ideal two-particle fluctuations,

$L^{(0)} := \pm G^> G^<$, defined as

$$\delta\hat{L}_{ijkl}^{(0)}(t) := \pm \{G_{il}^>(t) \delta\hat{G}_{jk}(t) + \delta\hat{G}_{il}(t) G_{jk}^<(t)\}. \quad (24)$$

Applying the PA (23) to Eq. (22) leads to the EOM for $\delta\hat{G}^{\text{PA}}$ of the form

$$i\hbar \frac{d}{dt} \delta\hat{G}_{ij}^{\text{PA}}(t) = [h^{\text{HF}}, \delta\hat{G}^{\text{PA}}]_{ij}(t) + [\delta\hat{U}^{\text{HF}}, G^<]_{ij}(t), \quad (25)$$

where we introduced the effective single-particle Hartree-Fock Hamiltonian and the operator of an effective single-particle Hartree-Fock potential induced by fluctuations,

$$h_{ij}^{\text{HF}}(t) := h_{ij}(t) \pm i\hbar \sum_{kl} w_{ikjl}^\pm(t) G_{lk}^<(t), \quad (26)$$

$$\delta\hat{U}_{ij}^{\text{HF}}(t) := \pm i\hbar \sum_{kl} w_{ikjl}^\pm(t) \delta\hat{G}_{lk}(t), \quad (27)$$

with the (anti-)symmetrized interaction tensor, w^\pm , defined as

$$w_{ijkl}^\pm(t) := w_{ijkl}(t) \pm w_{ijlk}(t). \quad (28)$$

However, when applying the PA, we find that exchange symmetries of the exact two-particle exchange-correlation function are broken, which are essential for energy conservation and the stability of numerical calculations. This problem can be overcome by considering, instead, symmetric two-particle fluctuations, i.e., by considering Eq. (19), instead of Eq. (16), in Eq. (14).

Figure 1 illustrates the connection between the nonequilibrium GW approximation and the PA, which we now briefly discuss. In the standard NEGF theory, the single-particle Green function satisfies the Keldysh-Kadanoff-Baym equations (KBEs), which include many-body correlations via the self-energy; see, e.g., Refs. [15,17]. The GW approximation describes these correlations in terms of the dynamically screened interaction W that itself obeys an equation of motion—the Dyson equation, involving the polarization function Π . However, the KBEs have the drawback of an unfavorable scaling of the numerical complexity with the number of time steps, N_t , which is cubic [even for the simpler second Born (SOA) self-energy].

This unfavorable scaling can be relieved by applying the generalized Kadanoff-Baym ansatz (GKBA) [40], second line Fig. 1. The GKBA propagates the Green functions G^\lessgtr only along the time diagonal, and reconstructs the time-off-diagonal Green function approximately. Within the Hartree-Fock GKBA (HF-GKBA), this is done using Hartree-Fock propagators, $G^{\text{R,HF}}$ [17,41,42]. While this indeed improves the scaling for SOA self-energies to $O(N_t^2)$, nevertheless, for the GW self-energy, the scaling remains $O(N_t^3)$.

Major progress of the scaling is achieved with the G1–G2 scheme (third line) [19–21], which constitutes an exact reformulation of the HF-GKBA. This is achieved by eliminating the self-energy in favor of the correlated part of the two-particle Green function, \mathcal{G} . This means that the collision integral in the time-diagonal equation for $G^<$, in which the self-energy appears, is equivalently expressed in terms of $\mathcal{G}(t)$, giving rise to coupled time-local equations for $G^<(t)$ and $\mathcal{G}(t)$ —the G1–G2 scheme—which possess linear scaling, $O(N_t^1)$, for all common self-energies.

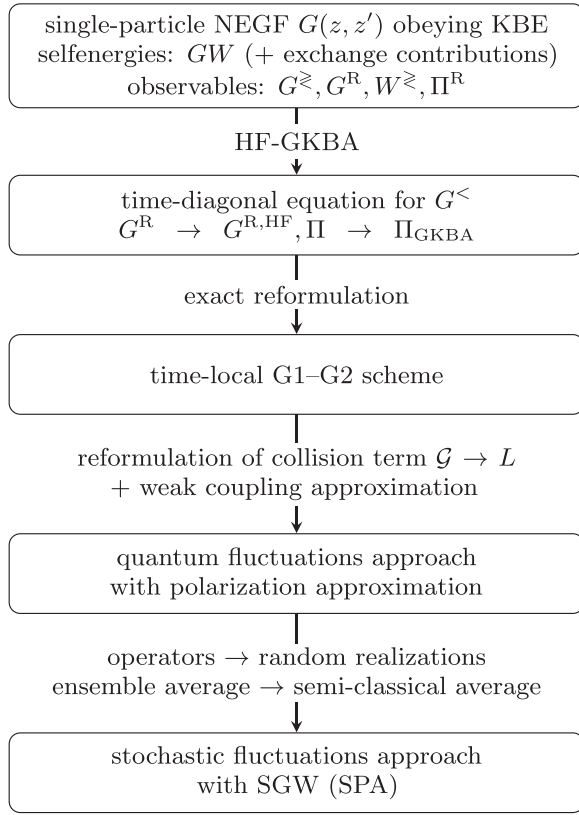


FIG. 1. Illustration of the steps to go from the Keldysh-Kadanoff-Baym equations (KBEs) using the GW approximation (with exchange contributions) to the time-local stochastic fluctuations approach using the SGW approximation (SPA). For details, see the text.

The remainder of Fig. 1 explains the quantum polarization approximation: As was shown in Ref. [24], it is equivalently possible to represent the collision term using two-particle fluctuations on the time diagonal. Using Eq. (23), the EOM for two-particle fluctuations then corresponds to the EOM for \mathcal{G} within the GW approximation including further exchange contributions ($w \rightarrow w^\pm$) in the case of weak coupling. Assuming instead

$$\delta \hat{L}_{ijkl}(t) \approx \pm \delta \hat{G}_{il}(t) G_{jk}^<(t) \quad (29)$$

leads to an EOM for L that corresponds to the GW approximation within the G1-G2 scheme in the weak-coupling regime. Further, the fluctuations approach offers the possibility for a combination with semiclassical stochastic methods, leading to the stochastic polarization approximation (SPA) and the stochastic GW approximation (SGW), respectively, which will be discussed in more detail Sec. III.

D. Quantum polarization approximation for two-time fluctuations

So far we considered the EOM (14) for $G^<$, which depends only on one-time two-particle fluctuations. Now we will consider the more general case that includes EOMs for the *two-time* two-particle fluctuations, as this allows for access to two-time observables that can be calculated from $L(t, t')$.

Using Eq. (25), we find for two-time two-particle fluctuations within the framework of the PA the following equations (dropping the superscript “PA”):

$$i\hbar \frac{\partial}{\partial t} L_{ijkl}(t, t') = [h^{\text{HF}}, L]_{ijkl}^{(1)}(t, t') + \pi_{ijkl}^{(1)}(t, t'), \quad (30)$$

$$i\hbar \frac{\partial}{\partial t'} L_{ijkl}(t, t') = [h^{\text{HF}}, L]_{ijkl}^{(2)}(t, t') + \pi_{ijkl}^{(2)}(t, t'), \quad (31)$$

where we introduced Hartree-Fock terms of the form

$$[h^{\text{HF}}, L]_{ijkl}^{(1)}(t, t') := \sum_p \{ h_{ip}^{\text{HF}}(t) L_{pjkl}(t, t') - h_{pk}^{\text{HF}}(t) L_{ijpl}(t, t') \}, \quad (32)$$

$$[h^{\text{HF}}, L]_{ijkl}^{(2)}(t, t') := \sum_p \{ h_{jp}^{\text{HF}}(t') L_{ipkl}(t, t') - h_{pl}^{\text{HF}}(t') L_{ijkp}(t, t') \}, \quad (33)$$

and the polarization terms

$$\pi_{ijkl}^{(1)}(t, t') := \pm i\hbar \sum_{pqr} L_{rjpl}(t, t') \{ w_{ipqr}^\pm(t) G_{qk}^<(t) - w_{qpk}^\pm(t) G_{iq}^<(t) \}, \quad (34)$$

$$\pi_{ijkl}^{(2)}(t, t') := \pm i\hbar \sum_{pqr} L_{iqkp}(t, t') \{ w_{pjqr}^\pm(t') G_{rl}^<(t') - w_{prl}^\pm(t') G_{jr}^<(t') \}. \quad (35)$$

As was discussed in Sec. II C, the PA is equivalent to the time-local GW approximation of the G1-G2 scheme, which includes additional exchange contributions. In fact, this equivalence also holds for the two-time extension considered herein. For this, we have to consider the EOMs of two-particle quantities. We will start from the Bethe-Salpeter equation (BSE) for the XC function on the Keldysh contour given by [37]

$$L_{ijkl}(z_1, z_2, z'_1, z'_2) = \pm G_{il}(z_1, z'_2) G_{jk}(z_2, z'_1) + \sum_{pqrs} \int_C G_{ip}(z_1, z_3) G_{rk}(z_5, z'_1) K_{pqrs}(z_3, z_4, z_5, z_6) L_{sjql}(z_6, z_2, z_4, z'_2) d(z_3, \dots, z_6), \quad (36)$$

where K denotes the two-particle irreducible vertex defined as

$$K_{ijkl}(z_1, z_2, z'_1, z'_2) := \frac{\delta \Sigma_{ik}(z_1, z'_1)}{\delta G_{lj}(z'_2, z_2)}, \quad (37)$$

i.e., as the functional derivative of the single-particle self-energy Σ with respect to the single-particle Green function G . Within the GW approximation, the vertex simplifies to

$$K_{ijkl}(z_1, z_2, z'_1, z'_2) \approx \pm i\hbar w_{ijkl}(z_1) \delta_C(z_1, z_2) \delta_C(z_1, z'_1) \delta_C(z_1, z'_2), \quad (38)$$

where δ_C denotes the delta distribution on the Keldysh contour. As illustrated in Fig. 2, upper box, this approximation for K in the BSE is equivalent to solving the KBE for the single-particle Green function with a properly chosen external field $U_{\text{ex}}(t)$ and the Hartree self-energy, $\Sigma \rightarrow \Sigma^{\text{H}}$ when considering the linearization of the equation in U_{ex} [14]. Moreover,

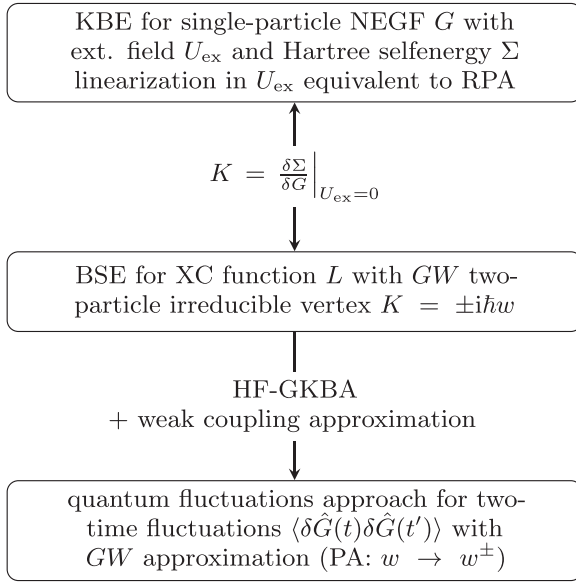


FIG. 2. Connection between three concepts: the KBE with Hartree self-energy and an external field, the BSE for the XC function [Eq. (36)] with two-particle irreducible vertex (38), and the present two-time quantum fluctuations approach [Eqs. (30) and (31)].

exchange contributions, which are included in the PA, can be considered by the replacement $w \rightarrow w^\pm$.

Now the question remains, how is the BSE related to the present two-time quantum polarization approximation (cf. the lower box in Fig. 2)? The result of a straightforward but lengthy analysis [43] is summarized as follows: Using the two-particle reducible vertex K^{red} , which obeys the following BSE [16]:

$$K_{ijkl}^{\text{red}}(z_1, z_2, z'_1, z'_2) = \pm K_{ijkl}(z_1, z_2, z'_1, z'_2) \sum_{pqrs} \int_C K_{ipkq}(z_1, z_3, z'_1, z_4) G_{qr}(z_4, z_5) G_{sp}(z_6, z_3) K_{rjkl}^{\text{red}}(z_5, z_2, z_6, z'_2) d(z_3, \dots, z_6), \quad (39)$$

it is possible to eliminate any dependence on the XC function on the right-hand side of Eq. (36), i.e., we have

$$L_{ijkl}(z_1, z_2, z'_1, z'_2) = \pm G_{il}(z_1, z'_2) G_{jk}(z_2, z'_1) \sum_{pqrs} \int_C G_{ip}(z_1, z_3) G_{jq}(z_2, z_4) K_{pqrs}^{\text{red}}(z_3, z_4, z_5, z_6) G_{rk}(z_5, z'_2) G_{sl}(z_6, z'_2) d(z_3, \dots, z_6). \quad (40)$$

Considering the real-time component of the XC function corresponding to two-time two-particle fluctuations and using the approximation (38) with $w \rightarrow w^\pm$ as well as applying the HF-GKBA then leads to Eqs. (30) and (31). Note that this agreement is restricted to the applicability range of both approaches, i.e., to weak coupling, beyond which also differences in the level of self-consistency become significant [44]. More details are given in Ref. [43].

E. Density response function and dynamic structure factor

There are a variety of observables that depend on fluctuations, which are generally not on the time diagonal, but depend on multiple (in general) independent time arguments. Two particularly important observables are the density response function and the dynamic structure factor. Here, we consider the (retarded) density response function, which, for an arbitrary basis, is defined as

$$\chi_{ij}^R(t, t') := i\hbar\Theta(t - t') \langle [\delta\hat{G}_{ii}(t), \delta\hat{G}_{jj}(t')] \rangle \quad (41)$$

$$= i\hbar\Theta(t - t') \{L_{ijij}(t, t') - L_{jiij}(t, t')\} \quad (42)$$

$$= -2\hbar\Theta(t - t') \text{Im}[L_{ijij}(t, t')], \quad (43)$$

where exchange symmetries of two-particle fluctuations were used, i.e., $L_{ijkl}(t, t') = [L_{lkji}(t', t)]^*$. Hence, the dynamics of χ^R in the PA is directly given by Eqs. (30) and (31) for two combinations of indices for which $\delta\hat{G}$ describes density fluctuations.

Considering a representation of the system in position space, i.e., $G_{ij}(t) \rightarrow G(\mathbf{r}, \mathbf{r}', t)$, we additionally introduce the center-of-mass and relative time and position, i.e.,

$$\tau := t_1 - t_2, \quad T := \frac{t_1 + t_2}{2}, \quad (44)$$

$$\mathbf{r} := \mathbf{r}_1 - \mathbf{r}_2, \quad \mathbf{R} := \frac{\mathbf{r}_1 + \mathbf{r}_2}{2}. \quad (45)$$

With this, two-particle fluctuations with $\mathbf{r}_1 = \mathbf{r}'_1$ and $\mathbf{r}_2 = \mathbf{r}'_2$ can then be expressed, equivalently, as

$$L(\mathbf{r}_1, \mathbf{r}_2, t_1, t_2) \rightarrow L(\mathbf{r}, \mathbf{R}, \tau, T). \quad (46)$$

Next, the dynamic structure factor is defined as the Fourier transform of the correlation function of fluctuations of the charge density (intermediate scattering function), i.e., we consider the Fourier transform of two-particle fluctuations with respect to the relative time and position

$$S(\mathbf{q}, \omega, \mathbf{R}, T) := \int \int_{-\infty}^{\infty} L(\mathbf{r}, \mathbf{R}, \tau, T) e^{i(\omega\tau - \mathbf{r}\cdot\mathbf{q})} d\tau d\mathbf{r}. \quad (47)$$

For systems in equilibrium, the dynamic structure factor does not depend on the center-of-mass time, T , where the same applies for spatially homogeneous systems with respect to the center-of-mass position, \mathbf{R} . Analogously, this applies also to the density response function in the general case.

In a similar manner, one can also define the response function and structure factor of spin density fluctuations, which, however, will not be considered in this work.

III. STOCHASTIC APPROACH TO THE QUANTUM FLUCTUATION DYNAMICS

A. General concept

The stochastic mean-field theory (SMF) was first introduced by Ayik [28] and later extended by Lacroix and many others; see, e.g., Refs. [29,30]. Here, quantum-mechanical operators are replaced by stochastic quantities, i.e., $\delta\hat{G}_{ij}(t) \rightarrow \Delta G_{ij}^\lambda(t)$, and the quantum-mechanical expectation value by the standard stochastic expectation value, i.e., $\langle \cdot \rangle \rightarrow \overline{(\cdot)}$. In practice, the stochastic expectation value is approximated by the arithmetic mean, where the superscript “ λ ” denotes a

random realization, each of which is generated for the initial state according to a statistical ensemble and then propagated in time. This allows operator equations, e.g., Eqs. (22) and (25), to be solved approximately. Effectively, this is done at the single-particle level and only involves simple mean-field dynamics. The solution of the many-body problem therefore essentially reduces to the construction of a probability distribution for the initial state, mean-field dynamics, and semiclassical averaging [29].

Replacing products of noncommuting operators with random variables, however, requires symmetrization of said products. The probability distribution describing the initial state at $t = t_0$ is then constructed in such a way that all symmetrized quantum-mechanical moments are equal to the semiclassical moments. For the case of an ideal (uncorrelated) state, the first two quantum-mechanical moments are given by

$$\langle \delta \hat{G}_{ij}(t_0) \rangle = 0, \quad (48)$$

$$L_{ijkl}(t_0) = \langle \delta \hat{G}_{ik}(t_0) \delta \hat{G}_{jl}(t_0) \rangle = -\frac{1}{\hbar^2} \delta_{il} \delta_{jk} n_j (1 \pm n_i), \quad (49)$$

with $n_i := \pm i \hbar G_{ii}^<(t_0)$. We underline that considering only an ideal initial state is not a restriction because a correlated initial state can be produced from an ideal state via the adiabatic switching method, e.g., Refs. [45,46]. It has to be noted, however, that no probability distribution exists that reproduces all symmetrized quantum-mechanical moments [47].

B. Stochastic polarization approximation

We now apply the SMF approach to the PA, i.e., Eq. (25), and we find the stochastic polarization approximation (SPA), which is of the form (we drop the superscript “SPA” below and imply that all further considerations within the framework of the SMF theory are done using the SPA)

$$i \hbar \frac{d}{dt} \Delta G_{ij}^\lambda(t) = [h^{\text{HF}}, \Delta G_{ij}^\lambda]_{ij}(t) + [\Delta U^{\text{HF},\lambda}, G^<]_{ij}(t), \quad (50)$$

where we introduced the SMF-analog of the effective single-particle Hartree-Fock potential induced by fluctuations, cf. Eq. (27),

$$\Delta U_{ij}^{\text{HF},\lambda}(t) := \pm i \hbar \sum_{kl} w_{ikjl}^\pm(t) \Delta G_{lk}^\lambda(t). \quad (51)$$

Applying the PA to the SMF theory leads to a neglect of any coupling to higher moments and thereby reduces the impact of choosing an approximate probability distribution for the initial state. In fact, extensive calculations within the framework of the Hubbard model indicate that all distributions are equivalent, provided they correctly describe the first two moments. Analogously, we can derive a stochastic version of the *GW* approximation (SGW) within the fluctuations framework for weak coupling [24].

The numerical scaling (CPU time and memory) of this approximation is proportional to the number of samples N_s . The CPU-time scaling of the SPA/SGW is given by $O(N_s N_b^4 N_t)$, where N_b is the number of basis states and N_t is the number of time steps. Due to this dependence, the specific choice of sampling allows for optimization and can make this approach advantageous compared to the G1–G2-*GW* approximation, which has a scaling of $O(N_b^6 N_t)$ [20].

C. Multiple ensembles approach

Although the SMF approach allows for a solution of certain operator equations and provides several other advantages compared to other methods, there are significant shortcomings of this theory that have to be addressed. The most striking is the semiclassical nature of the approach, i.e., the attempt to describe a quantum-mechanical system using a classical probability distribution. Even if the SPA restricts the number of significant moments, this stochastic approximation poses major limitations as quantum coherence effects cannot be properly accounted for, thus restricting this approach to weakly and moderately coupled systems. Additionally, this approach is unable to compute any observables that depend on the ordering of the underlying operators, e.g., the density response function, cf. Eq. (41). Here, we introduce a partial solution to this problem within the framework of the SPA (or equivalently any approximation to the fluctuations hierarchy that only takes into account the first two moments).

Basic ideas

The solution we propose is the multiple ensembles (ME) approach. Instead of considering only one statistical ensemble to describe realizations of the initial state, we consider two equivalent ensembles, and we replace quantum fluctuations according to

$$\delta \hat{G}_{ij} \rightarrow (\Delta G_{ij}^{(1),\lambda}, \Delta G_{ij}^{(2),\lambda}), \quad (52)$$

whereas products of operators are replaced based on their ordering:

$$\hat{L}_{ijkl} = \delta \hat{G}_{ik} \delta \hat{G}_{jl} \rightarrow \tilde{L}_{ijkl} := \Delta G_{ik}^{(1),\lambda} \Delta G_{jl}^{(2),\lambda}. \quad (53)$$

Analogously, we define the expectation value of two-particle fluctuations within the ME approach as

$$\tilde{L}_{ijkl}(t, t') := \overline{\tilde{L}_{ijkl}(t, t')}, \quad (54)$$

$$\tilde{L}_{ijk}(t) := \tilde{L}_{ijk}(t, t'). \quad (55)$$

Here, we see why this approach is restricted to approximations that only consider the first two moments. For example, the exact EOM for $\delta \hat{G}$, cf. Eq. (22), includes terms that are quadratic in $\delta \hat{G}$. These terms would then be replaced by scalar quantities, cf. Eq. (53), whereas all terms that are only linear in $\delta \hat{G}$ would be replaced by two component quantities, cf. Eq. (52). Additionally, we are unable to properly define third and higher moments within this approach. This is, however, not a problem within the framework of the SPA since higher moments are neglected, and all considered observables only depend on two-particle fluctuations, including the correlation energy and the density response function.

Since we do not require any additional symmetrization, by applying the ME, compared to standard SMF theory, the constraints for the initial state are given by replacing the operators in Eqs. (48) and (49) according to Eqs. (52)

and (53),

$$\overline{\Delta G_{ij}^{(1),\lambda}(t_0)} = \overline{\Delta G_{ij}^{(2),\lambda}(t_0)} = 0, \quad (56)$$

$$\overline{\Delta G_{ik}^{(1),\lambda}(t_0)\Delta G_{jl}^{(2),\lambda}(t_0)} = -\frac{1}{\hbar^2}\delta_{il}\delta_{jk}n_j(1 \pm n_i). \quad (57)$$

The single-particle fluctuation operator, $\delta\hat{G}$, obeys the symmetry

$$\delta\hat{G}_{ij} = -\delta\hat{G}_{ji}^\dagger. \quad (58)$$

Within the standard SMF approach, we construct the random variables so that this symmetry is preserved, i.e., $\Delta G_{ij}^\lambda = (-\Delta G_{ji}^\lambda)^*$. For the ME approach, however, we demand, instead, that the fluctuations obey the symmetry

$$\Delta G_{ij}^{(1),\lambda} \equiv -(\Delta G_{ji}^{(2),\lambda})^*. \quad (59)$$

Thus, the two newly defined ensembles reduce to a single random variable, and we define $\Delta G_{ij}^\lambda := \Delta G_{ij}^{(1),\lambda} \equiv -(\Delta G_{ji}^{(2),\lambda})^*$. Imposing this relation, therefore, we find for two-particle fluctuations within the ME approach,

$$\tilde{L}_{ijkl}(t, t') = [\tilde{L}_{lkji}(t', t)]^*, \quad (60)$$

thus reproducing one of the exchange properties of the exact two-particle fluctuations. Furthermore, Eqs. (56) and (57) take the following form:

$$\overline{\Delta G_{ij}^\lambda(t_0)} = 0, \quad (61)$$

$$\overline{\Delta G_{ik}^\lambda(t_0)[\Delta G_{lj}^\lambda(t_0)]^*} = \frac{1}{\hbar^2}\delta_{il}\delta_{jk}n_j(1 \pm n_i). \quad (62)$$

Again, we only consider the ME approach from this point onward, unless stated otherwise.

D. Semiclassical dynamics of the fluctuations

The dynamics of $G^<$ and ΔG^λ , within the ME approach, directly follow from Eqs. (14) and (25) with the symmetric collision term [cf. Eq. (19)],

$$i\hbar \frac{d}{dt} G_{ij}^<(t) = [h^H, G_{ij}^<(t)] + [S + S^\dagger]_{ij}(t) + [I^{\text{ME}} + I^{\text{ME}\dagger}]_{ij}(t), \quad (63)$$

$$i\hbar \frac{d}{dt} \Delta G_{ij}^\lambda(t) = [h^{\text{HF}}, \Delta G_{ij}^\lambda(t)] + [\Delta U^{\text{HF}}, G_{ij}^<(t)], \quad (64)$$

where we defined the ME-collision term, I^{ME} , as

$$I_{ij}^{\text{ME}}(t) := \pm \frac{i\hbar}{2} \sum_{klp} w_{iklp}(t) \{\tilde{L}_{plkj}(t) + \tilde{L}_{lpjk}(t)\}. \quad (65)$$

Notice that we again have to resort to symmetrized expressions (anticommutator) due to the symmetry breaking of the underlying approximation.

E. Sampling

The sampling methods for the ME approach are analogous to those of the standard SMF approach. Here, we focus on two approaches to sampling the initial state: stochastic and deterministic sampling that are briefly explained in the following.

1. Stochastic sampling

The standard approach for the construction of the initial state, within the standard SMF theory, is stochastic sampling. Here, known probability distributions, such as a Gaussian distribution or a uniform distribution, are chosen to reproduce the symmetric moments. For the ME approach, we consider a set of independent complex random variables $\Delta G_{ij}^\lambda(t_0)$ with zero mean and variance given by

$$\overline{|\Delta G_{ij}^\lambda(t_0)|^2} = \frac{1}{\hbar^2}n_j(1 \pm n_i). \quad (66)$$

As mentioned in Sec. III A, the expectation value is usually approximated by the arithmetic mean, i.e., a sufficiently large number of random realizations of the initial state is generated according to said constraints, cf. Eq. (66).

2. Deterministic sampling

In Ref. [24], a new sampling method was proposed for the special case of fermions at zero temperature [48]. The idea of the so-called “deterministic sampling” is to consider a system of nonlinear equations and construct a solution that exactly satisfies the properties of the initial state. The algorithm of Ref. [24] has to be adjusted only slightly for the ME approach. It follows that the system of nonlinear equations is given by

$$\sum_{\lambda=1}^M \Delta n_{ij}^\lambda = 0, \quad (67)$$

$$\sum_{\lambda=1}^M \Delta n_{ik}^\lambda (\Delta n_{lj}^\lambda)^* = M \delta_{il} \delta_{jk} \delta_{n_j,1} \delta_{n_i,0}, \quad (68)$$

with $\Delta n_{ij}^\lambda := -i\hbar \Delta G_{ij}^\lambda(t_0)$ and $M \in \mathbb{N}$. The parameter M has to be chosen such that a solution of the system of equations exists.

Here, we consider a fermionic system with spin configurations \uparrow, \downarrow [49] and assume spin symmetry of the initial state, i.e., $n_i^\uparrow = n_i^\downarrow$. Let $N_b \in \mathbb{N}$ denote the size of the basis for one spin component and $N_p, N_h \in \mathbb{N}$ denote the number of occupied and unoccupied orbitals, respectively, for one spin component, i.e., $N_p + N_h = N_b$. Without loss of generality, we assume $n_i^\uparrow = n_i^\downarrow = 1$ for $i = 1, \dots, N_p$ and $n_i^\uparrow = n_i^\downarrow = 0$ for $i = N_p + 1, \dots, N_b$. A solution to Eqs. (67) and (68) can be found analogously to Ref. [24] by setting $N_s = 4M = 4N_p N_h$ and

$$\Delta n^{\alpha\beta,\sigma} = \begin{pmatrix} 0 & \mathcal{A}^{\alpha\beta,\sigma} \\ 0 & 0 \end{pmatrix} \quad (69)$$

with $\mathcal{A}^{\alpha\beta,\sigma} \in \mathbb{C}^{N_h \times N_p}$. The matrix $\mathcal{A}^{\alpha\beta,\sigma}$ is of the form

$$\mathcal{A}_{ij}^{\alpha\beta,\uparrow} := \begin{cases} (-1)^\beta (M/2)^{1/2} & \text{for } \varphi(i, j) = \alpha, \beta \in \{1, 2\}, \\ 0 & \text{otherwise,} \end{cases} \quad (70)$$

$$\mathcal{A}_{ij}^{\alpha\beta,\downarrow} := \begin{cases} (-1)^\beta (M/2)^{1/2} & \text{for } \varphi(i, j) = \alpha, \beta \in \{3, 4\}, \\ 0 & \text{otherwise} \end{cases} \quad (71)$$

for $(\alpha, \beta) \in \{1, \dots, M\} \times \{1, \dots, 4\}$ and an arbitrary bijection $\varphi: \{1, \dots, N_p\} \times \{1, \dots, N_h\} \rightarrow \{1, \dots, M\}$. Using this approach for the construction of a solution, we only require a total of $8N_p N_h$ samples, thus deterministic sampling for the

ME approach has an advantageous numerical scaling compared to the standard deterministic sampling, which requires $16N_p N_h$ samples.

F. Application to the density response function and dynamic structure factor

We now apply the ME approach to the density response function, Eq. (41), and find

$$\chi_{ij}^{\text{R,ME}}(t, t') := -i\hbar\Theta(t - t') \left\{ \overline{\Delta G_{ii}^\lambda(t) [\Delta G_{jj}^\lambda(t')]^*} - \overline{[\Delta G_{ii}^\lambda(t)]^* \Delta G_{jj}^\lambda(t')} \right\} \quad (72)$$

$$= 2\hbar\Theta(t - t') \text{Im} \left[\overline{\Delta G_{ii}^\lambda(t) [\Delta G_{jj}^\lambda(t')]^*} \right] \quad (73)$$

$$= -2\hbar\Theta(t - t') \text{Im}[\tilde{L}_{ijij}(t, t')], \quad (74)$$

thus reproducing the result of Eq. (43).

Because we require the two ensembles to satisfy Eq. (59), realizations of single-particle fluctuations are not necessarily purely imaginary, thus implying that the imaginary part of products of fluctuations can be nonzero in general. If we required each ensemble to be anti-Hermitian, i.e., $\Delta G_{ij}^{(n),\lambda} = -(\Delta G_{ji}^{(n),\lambda})^*$, for $n \in \{1, 2\}$, the diagonal elements would be purely imaginary for arbitrary times. This implies that these products would be real, hence the retarded density response function would be purely imaginary. The exact density response function, however, is real [16].

Analogously to previous considerations, the dynamic structure factor follows within the ME approach, cf. Eq. (47). This multiple ensembles approach thus provides direct access to spectral two-particle quantities. In equilibrium, the result depends only on the time difference, τ . However, our approach remains fully valid in nonequilibrium, where the density response, in addition, depends on the center-of-mass time, T .

G. Application to the Fermi-Hubbard model

1. Hubbard Hamiltonian

For the Fermi-Hubbard model, the general pair-interaction of Eq. (2) transforms into

$$w_{ijkl}^{\alpha\beta\gamma\delta} = U\delta_{ij}\delta_{ik}\delta_{il}\delta_{\alpha\gamma}\delta_{\beta\delta}(1 - \delta_{\alpha\beta}), \quad (75)$$

with the on-site interaction U and the spin components being denoted by Greek indices. Additionally, the kinetic energy is replaced by a hopping Hamiltonian

$$h_{ij} = -\delta_{(i,j)}J, \quad (76)$$

which includes nearest-neighbor hopping, i.e., $\delta_{(i,j)} = 1$, if the sites i and j are adjacent, and $\delta_{(i,j)} = 0$, if they are not. The total Hamiltonian is then given by

$$\hat{H} = -J \sum_{(i,j)} \sum_{\sigma} \hat{c}_{i\sigma}^{\dagger} \hat{c}_{j\sigma} + U \sum_i \hat{n}_i^{\uparrow} \hat{n}_i^{\downarrow} + \hat{H}^x(t), \quad (77)$$

where \hat{H}^x describes a possible external excitation of the system. Here, we only consider one-dimensional chains and choose two types of excitations. The first is a potential “kick”

applied to the first site:

$$\hat{H}_I^x(t) = H_0(t - t_0)(\hat{n}_1^{\uparrow} + \hat{n}_1^{\downarrow}), \quad (78)$$

where $H_0(t - t_0)$ describes a narrow pulse at time $t = t_0$ with amplitude H_0 . The second is a confinement “quench” applied to the chain [18]:

$$\hat{H}_{II}^x(t) = V_0(t - t_0) \sum_{i=1}^M (\hat{n}_i^{\uparrow} + \hat{n}_i^{\downarrow}), \quad (79)$$

consisting of M connected sites where we will use $M = N/2$. At time $t = t_0$ the potential is switched off, which initiates a diffusion-type process.

2. Implementation of SPA-ME

The EOMs for the single-particle Green function and fluctuations in SPA-ME, Eqs. (63) and (64), take the following form:

$$i\hbar \frac{d}{dt} G_{ij}^{<,\sigma}(t) = [h^{\sigma}, G^{<,\sigma}]_{ij}(t) + [I + I^{\dagger}]_{ij}^{\sigma}(t), \quad (80)$$

$$i\hbar \frac{d}{dt} \Delta G_{ij}^{\lambda,\sigma}(t) = [h^{\sigma}, \Delta G^{\lambda,\sigma}]_{ij}(t) + [\Delta U^{\lambda,\sigma}, G^{<,\sigma}]_{ij}(t), \quad (81)$$

where the Hartree-(Fock) Hamiltonian and fluctuation Hartree-Fock potential in Eqs. (80) and (81) become, in the Hubbard basis (without external excitation),

$$h_{ij}^{\sigma}(t) := h_{ij}^{\text{HF},\sigma}(t) \equiv h_{ij}^{\text{H},\sigma}(t) = -\delta_{(i,j)}J - i\hbar\delta_{ij}U\bar{G}_{ii}^{\sigma}(t), \quad (82)$$

$$\begin{aligned} \Delta U_{ij}^{\lambda,\sigma}(t) &:= \Delta U_{ij}^{\text{HF},\lambda,\sigma}(t) \equiv \Delta U_{ij}^{\text{H},\lambda,\sigma}(t) \\ &= -i\hbar\delta_{ij}U\Delta G_{ii}^{\lambda,\bar{\sigma}}(t). \end{aligned} \quad (83)$$

Here, $\sigma = \uparrow (\downarrow)$ implies $\bar{\sigma} = \downarrow (\uparrow)$. This shows that all exchange contributions vanish due to the specific choice of the pair-interaction so that, in this case, the SPA is equivalent to SGW. The collision term in Eq. (80) takes the form

$$I_{ij}^{\sigma}(t) = -\frac{i\hbar}{2}U \{ \tilde{L}_{iii}^{\bar{\sigma}\sigma}(t) + \tilde{L}_{iij}^{\sigma\bar{\sigma}}(t) \}, \quad (84)$$

whereas the contributions due to symmetrization become

$$S_{ij}^{\sigma}(t) = \frac{1}{2}U G_{ij}^{\sigma}(t) = -S_{ij}^{\dagger,\sigma}(t). \quad (85)$$

Thus, symmetrization also does not lead to any additional contributions in the Hubbard basis. Including the external excitation, cf. Eq. (78), effectively leads to a modification of the on-site interaction of the form $U \rightarrow U + H_0(t - t_0)$, i.e., the on-site interaction U increases for the first site at $t = t_0$ by the amplitude H_0 .

The initial state of the system in the natural orbital basis of $n(t_0)$ is chosen such that

$$G_{ij}^{\sigma}(t_0) = -\frac{1}{i\hbar}\delta_{ij}n_i^{\sigma}, \quad (86)$$

$$\overline{\Delta G_{ij}^{\lambda,\sigma}(t_0)} = 0, \quad (87)$$

$$\overline{\Delta G_{ij}^{\lambda,\sigma}(t_0) [\Delta G_{lk}^{\lambda,\sigma'}(t_0)]^*} = \frac{1}{\hbar^2} \delta_{il} \delta_{jk} \delta_{\sigma\sigma'} \delta_{n_j^{\sigma}, 1} \delta_{n_i^{\sigma}, 0}. \quad (88)$$

Depending on the system's configuration, it becomes necessary to perform a transformation from the natural orbital basis to the Hubbard basis. This can be achieved by diagonalization of the Hamiltonian and the transformation of G and ΔG^λ using its eigenvectors.

In general, it is necessary to compute a nontrivial interacting ground state from which the externally driven dynamics starts. Here, this is done using the so-called “adiabatic switching method” [18] by replacing the on-site interaction U with a time-dependent interaction $U(t)$. Calculations then start at t_s with an uncorrelated ground state, with $U(t_s) = 0$. The on-site interaction is then increased monotonically and sufficiently slowly such that, at t_0 , the system is in a fully correlated ground state with $U(t_0) = U$.

Our main focus will be on the investigation of the density response function, χ^R [cf. Eq. (74)], which is, within the framework of the ME approach, given by

$$\chi_{ij}^{R,ME}(t, t') = -2\hbar\Theta(t - t') \sum_{\sigma\sigma'} \text{Im}[\tilde{L}_{ijj}^{\sigma\sigma'}(t, t')]. \quad (89)$$

By again considering the relative time τ and center-of-mass time T , the Fourier transform of the density response function with respect to τ is given by

$$\chi_{ij}^{R,ME}(\omega, T) = \int_{-\infty}^{\infty} \chi_{ij}^{R,ME}(\tau, T) e^{i\omega\tau} d\tau. \quad (90)$$

The spatial coordinate of a lattice site can be defined as $x_i := a_0 i$ for a one-dimensional chain, with a_0 denoting the characteristic distance of two adjacent sites [50]. Additionally, we now consider equilibrium and periodic boundary conditions (PBCs) so that there is no center-of-mass dependence for time and space. We then also consider a Fourier transform with respect to the spatial relative coordinate, i.e.,

$$\chi^{R,ME}(q, \omega) = \int \chi_{ij}^{R,ME}(\omega) e^{-iqr_{ij}} dr_{ij}, \quad (91)$$

with $r_{ij} := x_i - x_j$. Analogously, we calculate the dynamic structure factor for said system within the ME approach as

$$S^{ME}(q, \omega) = \sum_{\sigma\sigma'} \int \int_{-\infty}^{\infty} \tilde{L}_{ijj}^{\sigma\sigma'}(\tau) e^{i(\omega\tau - r_{ij}q)} d\tau dr_{ij}, \quad (92)$$

$$= -4 \text{Im}[\chi^{R,ME}(q, \omega)]. \quad (93)$$

A generalization to nonequilibrium and spatially inhomogeneous systems is straightforward but will not be considered here.

For the density response of a system in the ground state (or thermodynamic equilibrium) and the dynamic structure factor, we set $t' = t_0$ and propagate only $\Delta G_{ij}^{\lambda, \sigma}(t)$. The final step is the averaging over the realizations λ to calculate the two-particle fluctuations and all further observables.

A different approach to the calculation of the Fourier transform of the density response function as well as the dynamic structure factor is provided by considering a kick excitation of the system, e.g., to the first site, cf. Eq. (78), following the idea of Ref. [14] as this produces a spectrally broad excitation that excites all transitions that are quantum-mechanically allowed

[14,51]. In linear response, we then find

$$n_i(t) = \int_{t_0}^t \chi_{i1}^R(t - \bar{t}) H_0(\bar{t} - t_0) d\bar{t}, \quad (94)$$

$$\chi_{11}(\omega) = \frac{\tilde{n}_1(\omega)}{\tilde{H}_0(\omega)}, \quad (95)$$

where $\tilde{n}_i(\omega)$ and $\tilde{H}_0(\omega)$ denote the Fourier transforms of the density on site i and the kick excitation, respectively. The dynamic structure factor then also immediately follows, cf. Eq. (93).

As we are primarily interested in the Fourier transform of the density response function, we introduce a small exponential damping in the results of the time propagation with a factor of $e^{-\eta t}$ to mitigate the influence of the finite propagation length. Although this leads to a broadening of the spectral quantities, this allows for better comparability of the results. The damping constant is chosen such that $e^{-\eta t_{\max}} < 10^{-4}$, where t_{\max} denotes the maximum propagation time.

IV. NUMERICAL RESULTS

We now present numerical results within the stochastic polarization approximation, systematically extending the results of Ref. [24] to response functions. First, we consider the ground state and excitation properties of small Hubbard clusters without PBC, including the Hubbard dimer and a six-site system, where benchmarks against exact results are possible. We then turn in Sec. IV B to larger clusters containing 50 sites with PBC and compare results for the density response function and dynamic structure factor for SPA-ME and RPA. Finally, in Sec. IV C we study the nonequilibrium dynamics and density response of Hubbard clusters following a short external excitation and a confinement quench.

A. Test of the ME approach for small Hubbard clusters in the ground state

First, we consider a Hubbard dimer at half-filling without PBC. The peak positions of the Fourier transform of the retarded density response function correspond to energies of particle-hole excitations of the ground state. For the Hubbard dimer, there is only one dipole-allowed excitation from the ground state with an excitation energy of the form

$$\Delta E = \frac{U}{2} + \frac{\sqrt{U^2 + 16J^2}}{2}. \quad (96)$$

In Fig. 3 the Fourier transform of the ground-state result for the retarded density response function at site 1, $\chi_{11}(t)$, Eq. (89), is shown. Comparison with analytical results confirms that this quantity yields the excitation spectrum of the system which contains a single excitation with the energy ΔE , Eq. (96), which is exactly reproduced in the noninteracting case. Even for $U = 1.0J$ the result is in good agreement with the analytical benchmark with regard to the peak position. However, for the relative peak height, significant deviations are visible. As the squared modulus of $\chi^R(\omega)$ is proportional to the excitation amplitude, these results imply that SPA-ME overestimates the dipole-allowed transition probability.

In Fig. 4 the peak position of the density response function is analyzed in more detail over a broader range of coupling

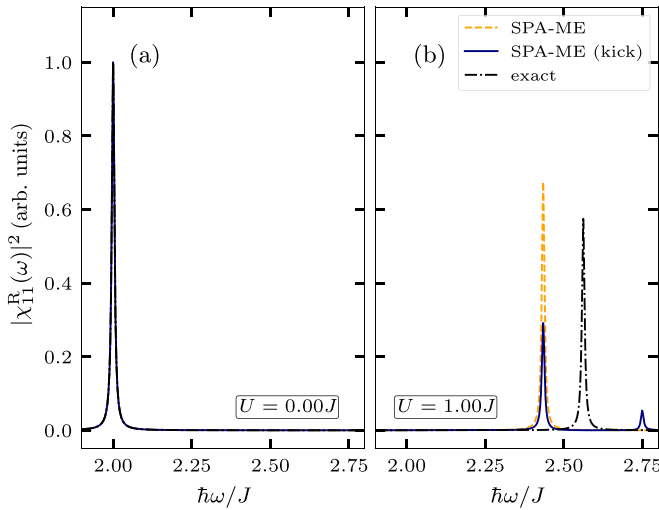


FIG. 3. Fourier transform of the density response function (arbitrary units) for the first site of a half-filled Hubbard dimer, without PBC, using SPA-ME with (blue lines) and without (orange lines) a kick excitation at $U = 0.0J$ (a) and $U = 1.0J$ (b). The results are compared to the Fourier transform of the analytical result. The damping constant was chosen to be $\eta = 0.005J/\hbar$.

parameters. There are only minor deviations from the exact result, for $U \lesssim 0.5J$. Not surprisingly, these deviations increase monotonically with increasing U/J since SPA is a weak-coupling approximation. Also, the functional form of the U -dependence deviates from the analytical solution, which increases faster than linear, whereas the slope of the SPA-ME result is sublinear.

Next, we extend the analysis to a larger system where the excitation spectrum contains more than one transition. We consider a half-filled six-site chain for the case of a noninteracting system ($U = 0.0J$) as well as for moderate coupling ($U = 1.0J$). For the noninteracting case we again find excel-

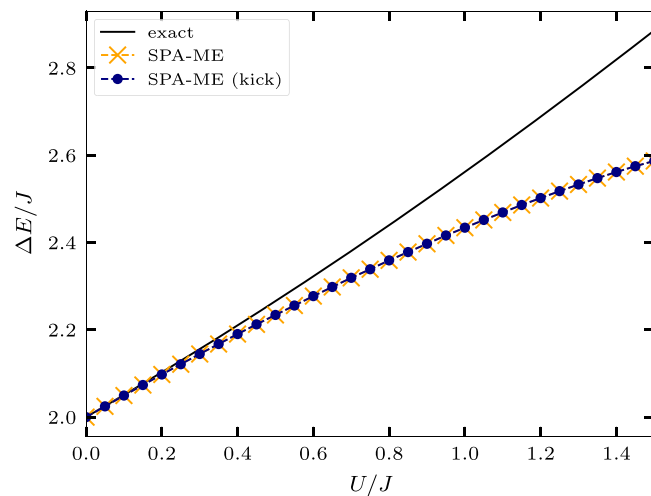


FIG. 4. Coupling dependence of the excitation energy of a Hubbard dimer for the dipole-allowed transition from the ground state, cf. Fig. 3. Comparison of the present SPA-ME simulations with (blue line) and without (orange line) a kick excitation to the analytical solution.

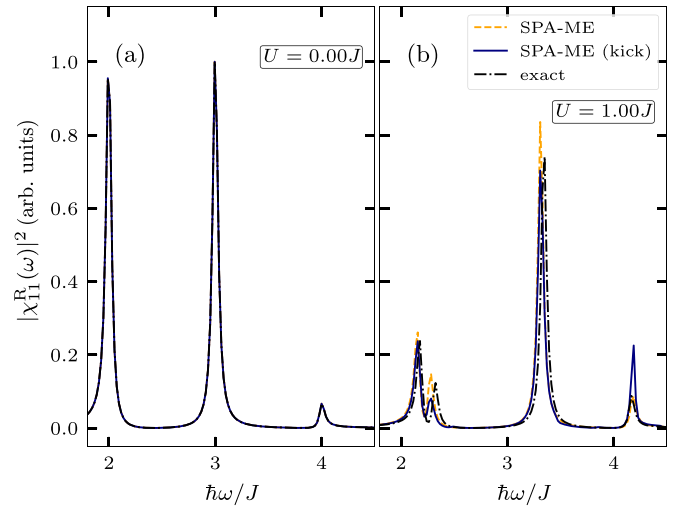


FIG. 5. Fourier transform of the density response function (arbitrary units) for the first site of a half-filled six-site system using SPA-ME with (blue lines) and without (orange lines) kick excitation at $U = 0.0J$ (a) and $U = 1.0J$ (b). The results are compared to an exact diagonalization (CI) calculation where a kick excitation, Eq. (78), was used. A damping constant of $\eta = 0.03J/\hbar$ for the exponential damping of the time propagation was used.

lent agreement between SPA-ME and the exact results, which were obtained from CI calculations. Moreover, differences are visible for moderate coupling. We see in Fig. 5 that the peak positions of the present SPA-ME calculations are in very good agreement with exact diagonalization results, however the peak height of the third peak shows significant deviations, which are less pronounced than for the dimer. The other peaks only display minor deviations and show good qualitative agreement. In general, we observe that the quality of our density response results improves with increasing system size.

B. Ground-state density response results for large Hubbard clusters

We now turn to larger Hubbard clusters. As an example, we consider a chain with periodic boundary conditions (i.e., a ring), which is half-filled with 50 sites for different coupling strengths. A similar simulation as for six sites, cf. Fig. 5, yields for the case of a 50-site ring a much more complex spectrum, which is shown in Fig. 6. We start with the case of a noninteracting system ($U = 0.0J$) at half-filling and observe excellent agreement with the analytical result for the tight-binding limit as the relative error is of the order of 10^{-6} .

Next, we consider in Fig. 7 the Fourier transform with respect to the spatial and time coordinate of the density response function from SPA-ME calculations. On the left side, the noninteracting system is displayed, while the right side shows the results for a moderately coupled system at $U = 1.0J$. Here, we see that the results for the noninteracting case for a finite system with PBC closely resemble the known results for the infinite chain [52]. The artificial damping of the time propagation leads to a broadening of the peaks due to the finite size of the system, thus causing them to merge into a continuous spectrum. At $U = 1.0J$ we see that the previously visible peaks start to vanish, whereas the main peaks are

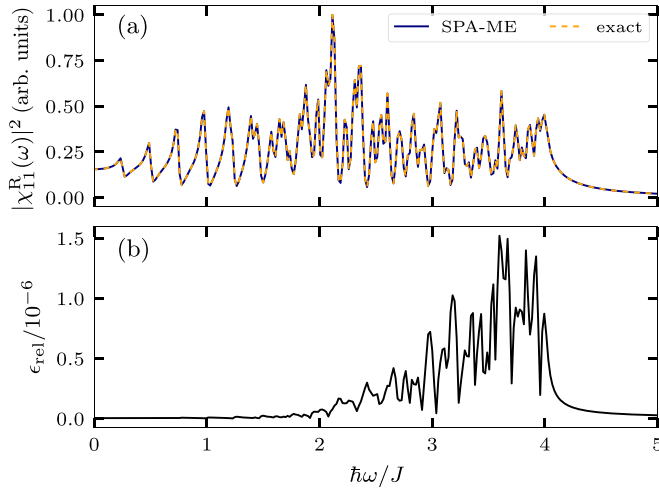


FIG. 6. (a) Fourier transform of the density response function (arbitrary units) for the first site of a half-filled 50-site ring at $U = 0.0J$ using SPA-ME. The results are compared to the analytical result. (b) Relative error of the Fourier-transformed density response. A damping constant of $\eta = 0.02J/\hbar$ was used.

slightly shifted upwards. Additionally, Fig. 7 displays the lines of the main peaks for the density response function obtained from RPA calculations. Here, we see that there is excellent agreement between the two approximations with regard to the chosen representation. This comparison of SPA-ME and RPA is further extended in the following.

We now consider the dynamic structure factor of the same system but for varying interaction strengths and specific wave numbers, and we closely compare results from SPA-ME to RPA calculations. What should we expect from this comparison? The answer has been given in the context of Fig. 2: On the one hand, the RPA of linear-response theory is equivalent to the BSE with a GW kernel, Eq. (38). On the other

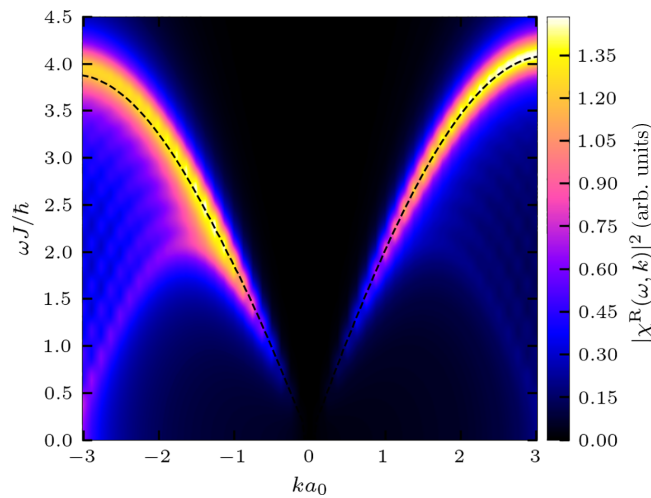


FIG. 7. Fourier transform of the density response function (arbitrary units) of a half-filled 50-site ring at $U = 0.0J$ (left) and $U = 1.0J$ (right) using SPA-ME. The dashed lines denote the corresponding peak positions from RPA calculations. A damping constant of $\eta = 0.2J/\hbar$ was used.

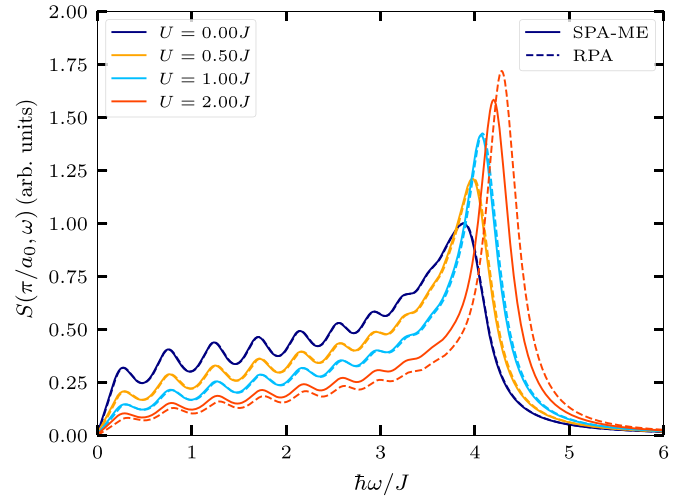


FIG. 8. Dynamic structure factor of a half-filled 50-site ring at $q = \pi/a_0$ for different U using SPA-ME (solid lines) and RPA (dashed lines).

hand, the two-time PA for L is equivalent to the same BSE approximation. Thus, the only remaining questions are how well the present SPA-ME approach combined with the semi-classical averaging procedure reproduces the PA, and thus the GW-BSE, and what effects do the different levels of self-consistency have; cf. the discussion in Sec. II D. With the present numerical results, we directly answer this question. The time-dependent SPA-ME results are multiplied by a factor of $e^{-\eta t}$ with damping constant $\eta = 0.2J/\hbar$, and the same damping constant, η , is used for the RPA calculations; see Eqs. (B2) and (B3). This is done to broaden the δ -like peaks due to the finite system size and better comparability to the infinite chain.

First, we consider the dynamic structure factor for a fixed wave number $q = \pi/a_0$ for different interaction strength. Figure 8 shows that there is excellent agreement between the SPA-ME and RPA results for weak coupling. With increasing interaction strength, deviations become more pronounced, however only for $U = 2.0J$ are significant differences between the two approximations visible. As both approximations are only applicable within the weak-coupling regime, this coupling strength is beyond their validity anyway. Moreover, both approximations show a main peak located at $\omega \sim 3.9J/\hbar$ for $U = 0.0J$ with $S \sim 1.0$ a.u. With increasing interaction strength, this peak is shifted towards higher frequencies ($\omega \sim 4.2J/\hbar$) and height with $S \sim 1.6$ a.u. at $U = 2.0J$, where the RPA peak is shifted to slightly higher frequencies compared to the SPA-ME peak ($S \sim 1.7$ a.u. at $\omega \sim 4.3J/\hbar$). These differences are explained by the use of ideal Green functions in the analytical RPA result, cf. Appendix B, whereas the SPA-ME involves correlated Green functions. Additionally, we observe that, due to the finite system size, there are a number of peaks visible next to the main peak which do not exist in the infinite chain. These peaks become less pronounced with increasing interaction strength. Here, the RPA results deviate, for $U = 2.0J$, from the SPA-ME results in that there is a slightly larger downward shift visible for the peak height.

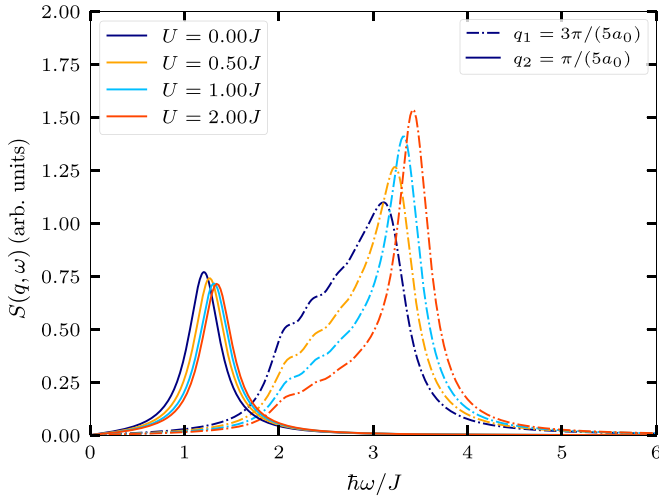


FIG. 9. Dynamic structure factor of a half-filled 50-site ring at $q_1 = 3\pi/(5a_0)$ (solid lines) and $q_2 = \pi/(5a_0)$ (dash-dotted lines) for different U using SPA-ME.

Next, we consider in Fig. 9 the dynamic structure factor for two different wave numbers, $q_1 = 3\pi/(5a_0)$ and $q_2 = \pi/(5a_0)$, at different U , using only SPA-ME. For q_2 we see that only a single peak is visible for each U located at $\omega \sim 1.2J/\hbar$ with a height of $S \sim 0.77$ a.u. while none of the other peaks due to the finite system size are present. With increasing interaction strength, a slight downward shift of the peak height is observed, in contrast to the previous results. Again, however, the peak position is shifted towards higher frequencies. Here, both shifts are not as pronounced as for the previous case. This changes for q_1 , where the position of the main peak is shifted from $\omega \sim 3.1J/\hbar$ to $\omega \sim 3.4J/\hbar$, thus displaying a stronger shift compared to the case $q = \pi/a_0$. Additionally, here the buildup of the finite-size peaks is observed. However, the peak height is shifted significantly downward, compared to q_1 and even $q = \pi/a_0$. Moreover, the peaks become less pronounced with increasing interaction strength so that they are barely visible for $U = 2.0J$. Lastly, the height of the main peak at $U = 0.0J$ is located at $S \sim 1.1$ a.u. and shifted upwards to $S \sim 1.5$ a.u. at $U = 2.0J$.

C. Nonequilibrium density response following an external kick excitation of a single site

After computing the density response for a system in the ground state, we now turn to the time-dependent density response following a rapid weak external perturbation (“kick”). Here, we again consider two approaches: first, computation of the density response function from a ground-state calculation with subsequent calculation of the density response in linear-response theory according to Eq. (94). The second approach is a direct nonequilibrium calculation following the external kick perturbation of the first site, cf. Eq. (78).

Let us first return to Fig. 3, where the present kick results have been included. Here, we see that, for the noninteracting case, the results from the nonequilibrium SPA-ME calculation agree with both the analytical and the equilibrium SPA-ME results. However, for the moderately coupled system we observe significant deviations, as an additional peak at $\omega = 2.75J/\hbar$

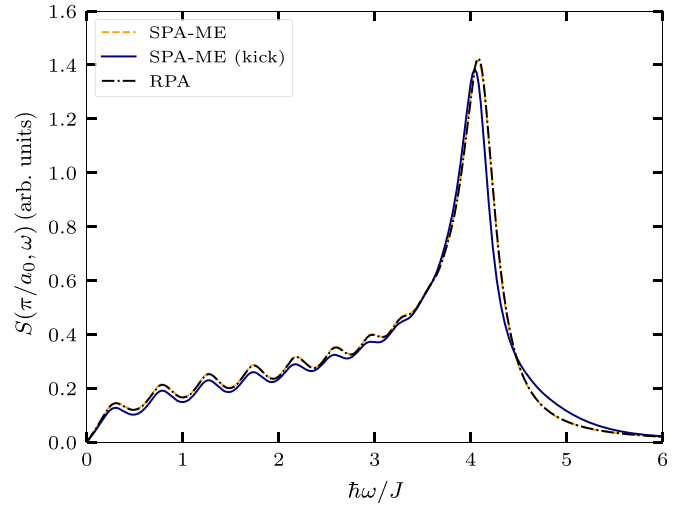


FIG. 10. Dynamic structure factor for a half-filled 50-site ring at $U = 1.0J$ at $q = \pi/a_0$ from SPA-ME with (blue line) and without (orange line) a kick excitation and RPA. The time propagated results were exponentially damped with damping constant $\eta = 0.2J/\hbar$.

appears. This effect is known from NEGF calculations [51]. Moreover, we see that the peak position of the equilibrium approach is well reproduced by one of the peaks from the nonequilibrium calculation. This trend is also visible when considering other interactions strengths, as shown in Fig. 4. Here, we see only minor deviations between the two approaches. Nonetheless, the height of the main peak shown in Fig. 3 is significantly reduced for the kick results.

Similar behavior is observed for the six-site chain shown in Fig. 5. Here, we also see that the peak positions are well reproduced by the nonequilibrium simulations. However, significant deviations of the heights of most peaks are visible, suggesting that the nonequilibrium scenario modifies the transition probabilities of almost all allowed transitions. We observe that, in contrast, the equilibrium results are significantly closer to the amplitudes of the exact solution.

In Fig. 10 we again consider the dynamic structure factor of a 50-site ring. At $U = 0.5J$ for a wave number $q = \pi/a_0$, we see the aforementioned excellent agreement of the equilibrium SPA-ME and RPA results. The nonequilibrium SPA-ME calculations display minor deviations compared to the other approaches. Here, the former are shifted slightly downward, for frequencies $\omega \lesssim 3.0J/\hbar$. Additionally, we see that the position of the main peak is shifted towards a smaller frequency with reduced peak height. For larger frequencies ($\omega \gtrsim 4.7J/\hbar$) we observe an increase of the nonequilibrium results compared to the other approaches, which is more pronounced compared to the aforementioned shift for smaller frequencies. A possible explanation of these deviations is that nonequilibrium simulations are known to capture correlation effects [14], but whether this applies to the present excitation requires further investigation; see also Sec. V.

Next, we again consider a half-filled six-site chain for different interaction strengths ($U/J = 0.0, 0.5, 1.0$) and compare the time-dependent density perturbation at the first site for SPA-ME, from linear-response theory and the kick

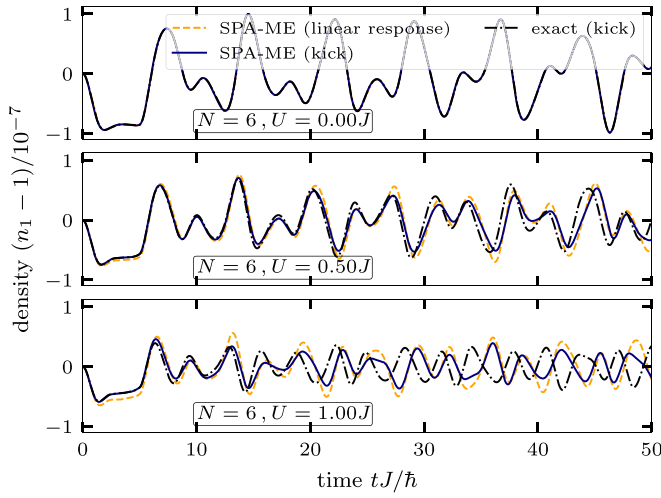


FIG. 11. Time-dependent density perturbation at the first site for a half-filled six-site chain for three coupling strengths [$U = 0.0J$ (a), $U = 0.5J$ (b), and $U = 1.0J$ (c)] following a kick excitation using SPA (blue lines) and CI. The data are compared to linear-response results from a ground-state SPA-ME calculation (orange lines); cf. Eq. (94).

excitation, to CI results. Figure 11(a) shows that in the noninteracting case, both SPA-ME results from linear response and nonequilibrium agree perfectly with the CI data. In (b) we still see good qualitative agreement of both calculations with the CI data, with deviations starting to increase for $t \gtrsim 20\hbar/J$. The linear-response results overestimate the amplitude of the oscillations compared to the nonequilibrium calculation. For the moderately coupled system with $U = 1.0J$ we immediately see in (c) that deviations between the results arise. The nonequilibrium SPA-ME results display better agreement with the exact result for longer times ($t \sim 7\hbar/J$) compared to the linear-response results ($t \sim 1\hbar/J$). Both, however, fail to accurately reproduce the oscillating behavior of the exact result for times larger than $\sim 20\hbar/J$ as there appears to be a time-dependent phase shift.

D. Nonequilibrium density response following a confinement quench

As a final nonequilibrium setup, we consider a confinement quench [18,53] of a half-filled system; cf. Eq. (79). This means the initial state is such that the left half of the sites is fully occupied while the right half is empty. Subsequently, at time $T = 0$, the confinement potential is removed suddenly, resulting in a rapid expansion of particles in the chain similar to a classical diffusion setup. Thus, immediately after the quench, the system is in strong nonequilibrium, providing an interesting test-bed for our ME approach. In particular, we are interested at this point in the density response during the relaxation process. Again, we start with a small system containing six sites with periodic boundary conditions and compare results of SPA-ME with those of exact diagonalization. In Fig. 12, we present the two-time nonequilibrium density response function for the half-filled ring at an interaction strength of $U = 0.1J$ obtained from the present SPA-ME model. Recall that the Heaviside function in the definition of

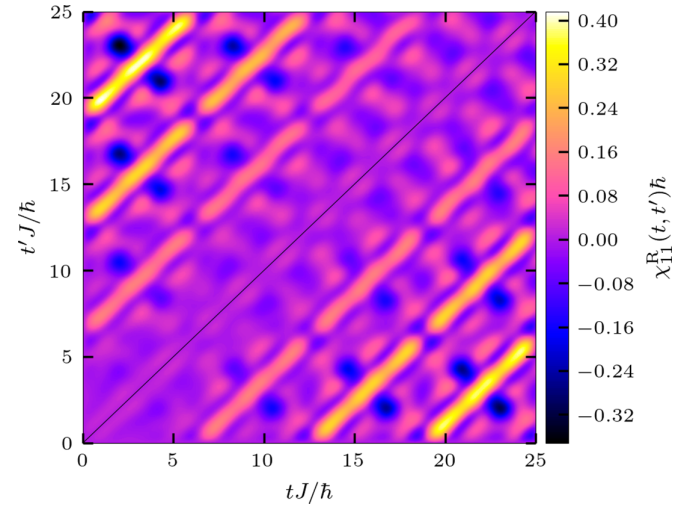


FIG. 12. Density response function for a half-filled ring with six sites at $U = 0.1J$ following a confinement quench at $t = 0$. Upper left (lower right) triangle corresponds to SPA-ME (CI) results.

the retarded component leads to $\chi_{ij}^R(t, t') \equiv 0$ for $t' > t$, cf. Eq. (43). This allows us to plot in the half-plane below the diagonal (black line) the corresponding CI result for the density response function $\chi_{ij}^R(t', t)$ for the transposed arguments. Obviously, there is very good agreement between the two results. We now move on to stronger coupling, $U = 0.4J$. The results are presented in Fig. 13, where significant differences between the two results are visible. It is noticeable here that the same trends are present for both results with respect to the phase of the oscillations. However, deviations in their amplitudes are visible. Moreover, we observe that the oscillations for the exact result are damped with increasing relative time, while the SPA-ME results illustrate the opposite trend. Comparing the results for the two interaction strengths, we notice that they differ mainly in the amplitude of the oscillations.

For a better comparison of the CI and SPA-ME data, we now present the results in 2D plots. There we show the density response function versus relative time, τ , for

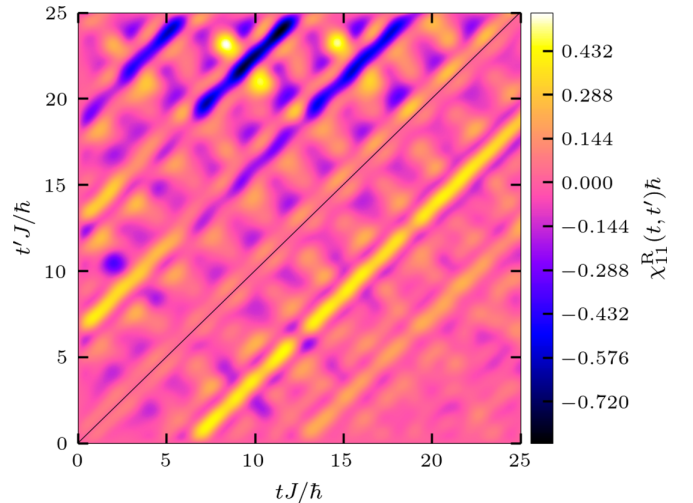


FIG. 13. Same as Fig. 12, but at $U = 0.4J$.

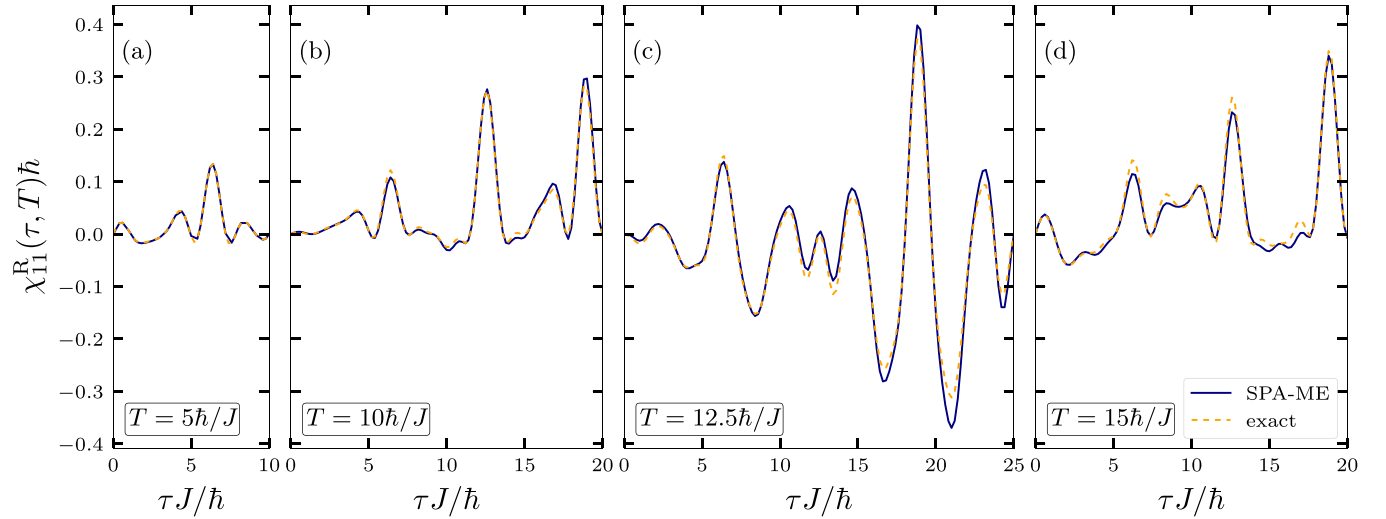


FIG. 14. Density response function for different times T following a confinement quench, for a half-filled ring with six sites at $U = 0.1J$. Comparison of the present SPA-ME approach to CI calculations.

fixed values of the center-of-mass time, T . In Fig. 14 we consider the density response function for four values of T for the case of weak coupling, $U = 0.1J$. Here, we see only minor deviations of the SPA-ME result from CI. The differences become more pronounced for $T = 12.5\hbar/J$ for oscillations with large amplitude, i.e., for $\tau \sim 20\hbar/J$. Further, we observe in the course of the relaxation process that there is a change in the frequencies of the oscillations. Additionally, as the propagation time increases, there is an increase in the amplitudes of the oscillations, with this trend continuing until $T = 12.5\hbar/J$ and then being reversed.

For $U = 0.4J$ (see Fig. 15) we observe the previously mentioned deviations of the SPA-ME result from the CI data. Only for $T = 5\hbar/J$ is good agreement visible. Already for $T = 10\hbar/J$ this holds only up to a relative time of $\tau = 5\hbar/J$. Afterwards, we observe that there is a shift of the phase of

the oscillations, where significant deviations in the amplitude increase. In particular, while the exact result shows a damping of the oscillatory behavior, the SPA-ME shows the opposite trend. This behavior is also observed in a stronger form for later center-of-mass times. It is noticeable that the minima of the density response function are shifted downward for the SPA-ME with increasing center-of-mass time, while there is no significant increase in the maxima. The observed damped behavior of the exact dynamics of the density response function at $U = 0.4J$ is also found for the density evolution shown in Fig. 16(b). Here, we again observe that SPA-ME overestimates the oscillations while still reproducing the exact phase. In (a) we see excellent agreement of the SPA-ME and exact results similar to the observed agreement for the density response function.

Finally, we turn again to larger systems for which, however, no CI data are available for comparison. Specifically,

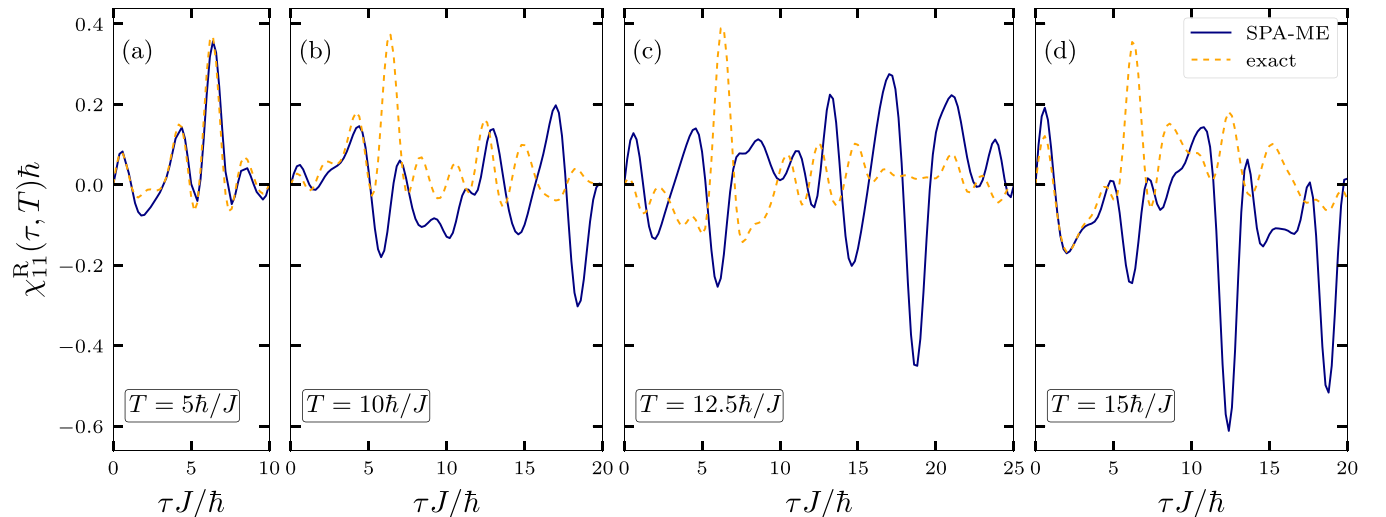


FIG. 15. Same as Fig. 14, but at $U = 0.4J$.

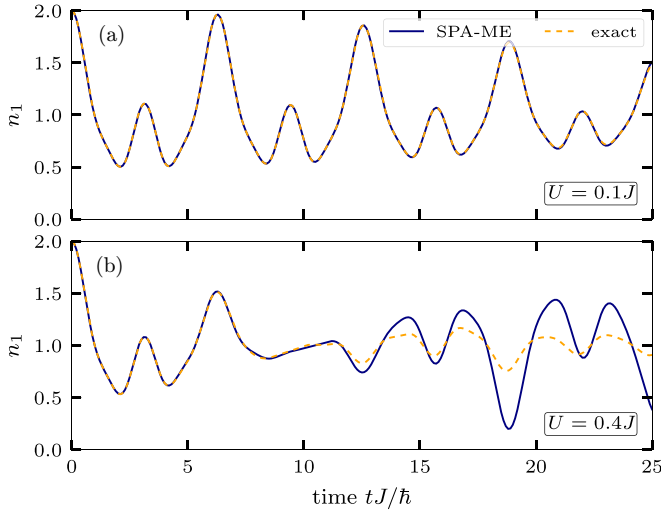


FIG. 16. Density evolution at site 1 of a half-filled ring with six sites following a confinement quench.

we consider a half-filled ring with 30 sites at $U = 0.1J$ and $0.4J$, respectively, following an analogous confinement quench. Figure 17 displays the density response function versus relative time for fixed center-of-mass times. Here, we see for $T = 5\hbar/J$ that the oscillations of the density response function are damped with increasing relative time. Moreover, we find that the phases of the oscillations are the same for both on-site interaction strengths, which is also observable for all later center-of-mass times with only minor deviations between the two. Again, we find that stronger coupling leads to an increase of the amplitude. However, there is no damping of the oscillations for either coupling strength for larger center-of-mass times.

Lastly, we consider nonequilibrium density response spectra of the same system at $U = 0.1J$ and $0.4J$, for large center-of-mass times, $T \geq 75$, which are shown in Fig. 18. These nonequilibrium spectra are obtained via Fourier trans-

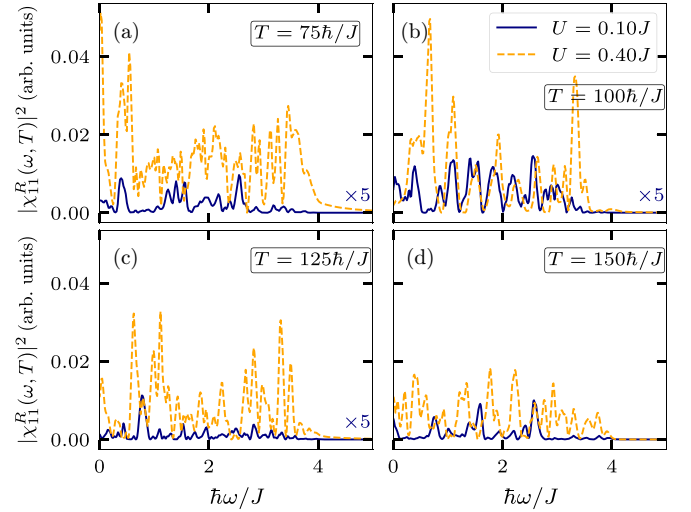


FIG. 18. Fourier transform of the density response function with respect to the relative time for a half-filled ring with 30 sites at fixed center-of-mass times, T , at $U = 0.1J$ and $0.4J$ using SPA-ME. The $U = 0.1J$ results in (a), (b), and (c) have been multiplied with a factor of 5. A damping constant of $\eta = 0.04J/\hbar$ was used.

form of the density response function with respect to the relative time τ for fixed center-of-mass times T . Here, we see a relatively similar structure of the spectra for both on-site interactions for $T = 100\hbar/J$. However, the transition probabilities are significantly larger for $U = 0.4J$ than for $U = 0.1J$ for all center-of-mass times. Additionally, we find that the transition probabilities for excitations are largest for $T = 150\hbar/J$ at $U = 0.1J$ compared to the other center-of-mass times, whereas this is the case for $T = 100\hbar/J$ at $U = 0.4J$.

Finally, we inquire whether the nonequilibrium spectra, for later times T , begin to approach the ground-state spectra. To this end, we have computed ground-state results for the same system that are displayed in Fig. 19. A first observation is that the nonequilibrium transition probabilities are significantly

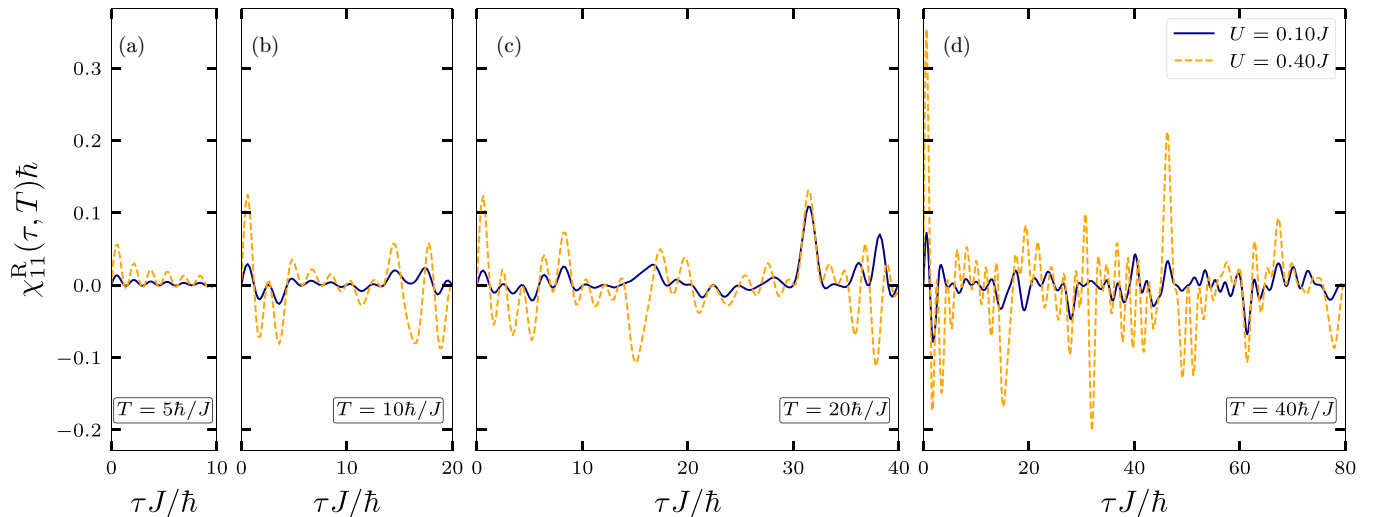


FIG. 17. Density response function for different center-of-mass times T following a confinement quench, for a half-filled ring with 30 sites at $U = 0.1J$ and $0.4J$ using SPA-ME.

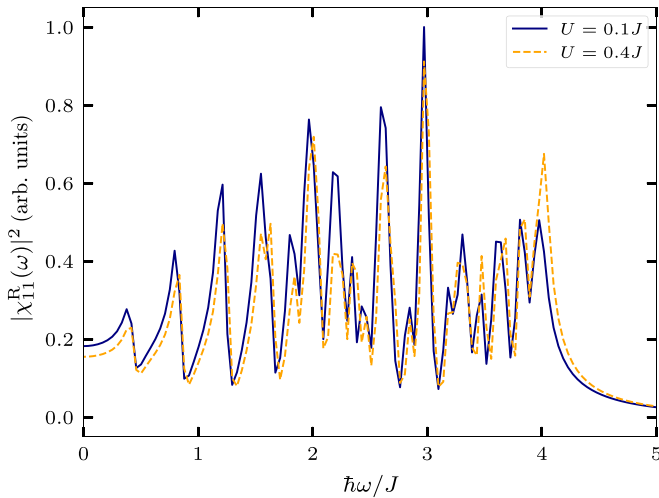


FIG. 19. Same as Fig. 18, but for the ground state at $U = 0.1J$ and $0.4J$.

smaller than their ground-state counterparts. Moreover, we find that the overall structure of the nonequilibrium spectra for $T = 150\hbar/J$ starts to resemble the ground-state spectra, at least for $U = 0.4J$. Similarly to the ground-state results, the nonequilibrium spectra also vanish for frequencies larger than $4J/\hbar$. Clearly, for a better quantitative comparison, longer nonequilibrium simulations would be desirable, as well as a comparison to equilibrium spectra at a finite temperature that takes into account the quench energy. This analysis is a subject of ongoing work.

V. DISCUSSION AND OUTLOOK

In this paper, we have extended our recent work on a novel quantum fluctuations approach presented in Ref. [24]. This approach starts from single-time single-particle density matrix operators and investigates their fluctuations around their expectation value—the single-particle density matrix (or time-diagonal Green function). The approach is conceptionally similar to the classical fluctuations approach of Klimontovich [25,27] as well as the stochastic mean field approximation of Ayik, Lacroix, and others [28–30]. All these methods have the attractive feature that correlation effects are mapped onto the dynamics of an ensemble of fluctuating single-particle quantities, and quantum expectation values are replaced by semiclassical mean values.

The advantage of the present approach is that it starts directly from the equations of motion for the nonequilibrium Green functions (NEGFs), which allows us to use well-known many-body approximations for the self-energy; for reference, e.g., see [16,17,46]; see also Fig. 1. This also allows us to use results from recent dramatic accelerations of NEGF simulations that were achieved by using the Hartree-Fock GKBA and its transformation to time-local equations—the G1–G2 scheme [19–21,54]. There the gain in computation speed comes at the price of storing the nonequilibrium two-particle Green function \mathcal{G}_2 , the size of which rapidly increases with the system size. One way to reduce the basis dimension is an embedding approach [23]. On the other hand, the present

quantum fluctuations approach is even more powerful as it avoids the computation of \mathcal{G}_2 in favor of single-particle fluctuations $\delta\hat{G}_{ij}(t)$ and their classical counterparts $\Delta G_{ij}^\lambda(t)$. This method was shown to accurately reproduce G1–G2 simulations for single-time quantities within the nonequilibrium GW approximation [24].

In this paper, we presented a major extension of the quantum fluctuations approach to two-time observables that are composed of single-particle fluctuations: the general two-time exchange-correlation function $L_{ijkl}(t, t')$, the density correlation function $\chi_{ij}^R(t, t')$, and the dynamic structure factor $S(q, \omega)$. To achieve this goal, we first developed the multiple ensembles idea, which allows one to compute commutators within the present semiclassical approach. This has led to the multiple ensembles stochastic polarization approximation (SPA-ME), which was extensively tested for Fermi-Hubbard chains in the numerics part of the paper. The first tests were devoted to the density response in the ground state. As we have shown in Fig. 2, the polarization approximation is, in the weak-coupling limit, equivalent to (a) the GW approximation of Bethe-Salpeter theory and (b) the random phase approximation of linear-response theory. Indeed, we demonstrated excellent numerical agreement of our SPA-ME results with the RPA, within the validity range of the approximation, i.e., for $U/J \lesssim 1$. From this we conclude that the SPA-ME very accurately reproduces the polarization approximation and that the observed differences for the SPA-ME and RPA for stronger coupling are most likely attributed to the use of ideal Green functions in the analytical RPA result, cf. Appendix B, whereas the SPA-ME involves correlated Green functions.

The main advantage of the present approach is its general applicability to correlated quantum systems in nonequilibrium. We demonstrated this for two types of external excitation: The first was a rapid potential kick applied to one site of the system. The second was a confinement quench in a system that was initially doubly occupied in its central region and then expands towards half-filling. In both cases, the SPA-ME approach allowed us to study the buildup of the nonequilibrium density response $\chi^R(\tau, T)$ as a function of physical time T that has passed after the excitation. Performing benchmarks against CI simulations, for small systems, we concluded that for weak coupling the method is very accurate. With increasing coupling, only the main features of the nonequilibrium spectra are captured, as expected from a weak-coupling approximation. We then turned to larger systems for which our method is expected to be more accurate [24].

Based on these first proof-of-principle results, we conclude that the present SPA-ME approach can be successfully applied to large systems for which the nonequilibrium density response and the impact of correlation effects can be studied for long propagation times. Work on a more systematic analysis of the nonequilibrium dynamics, both linear and nonlinear, and its dependence on the coupling strength and excitation scenario is presently in progress. A particularly interesting excitation scenario is to use a short spatially monochromatic pulse. As was shown in Ref. [14], nonequilibrium GW-KBE simulations of a uniform system following such an excitation are expected to yield high-quality dynamic structure factors

that are sum rule preserving and include vertex corrections, thereby going well beyond the RPA, cf. Fig. 2. Therefore, it can be expected that a similar scenario applied within the polarization approximation for $L(t, t')$ or, equivalently, within our SPA-ME scheme will also produce highly accurate correlated response properties for large systems that are out of reach for exact simulations.

ACKNOWLEDGMENT

We acknowledge stimulating discussions with Christopher Makai. This work is supported by the Deutsche Forschungsgemeinschaft via Project No. BO1366/16.

APPENDIX A: ANALYTICAL RESULT FOR THE DENSITY RESPONSE FUNCTION OF NONINTERACTING HUBBARD CLUSTERS

The Hamiltonian of a 1D tight-binding chain with periodic boundary conditions is given by

$$\hat{H}_0 = -J \sum_{\langle n, m \rangle} \sum_{\sigma} \hat{c}_{n\sigma}^{\dagger} \hat{c}_{m\sigma}, \quad (\text{A1})$$

where only chains with $N \in 4\mathbb{N} - 2$ sites will be considered. By transforming into the momentum basis

$$\hat{c}_{m\sigma}^{\dagger} = \frac{1}{\sqrt{N}} \sum_q e^{iqm} \hat{c}_{q\sigma}^{\dagger}, \quad (\text{A2})$$

$$\frac{q}{\pi/N} = -N, -N+2, \dots, N-2, \quad (\text{A3})$$

Eq. (A1) takes the form

$$\hat{H}_0 = -2J \sum_{q, \sigma} \cos(q) \hat{c}_{q\sigma}^{\dagger} \hat{c}_{q\sigma}, \quad (\text{A4})$$

where the time-dependent version of the field operators is given by

$$\hat{c}_{q\sigma}(t) := e^{-\frac{2iJ}{\hbar} \cos(q)t} \hat{c}_{q\sigma}. \quad (\text{A5})$$

From this we obtain the diagonal elements of the density operator for site m ,

$$\hat{n}_{m\sigma}(t) = \hat{c}_{m\sigma}^{\dagger}(t) \hat{c}_{m\sigma}(t) = \frac{1}{N} \sum_{q, q'} e^{i(q-q')m} \hat{c}_{q\sigma}^{\dagger}(t) \hat{c}_{q'\sigma}(t), \quad (\text{A6})$$

and the commutator

$$\begin{aligned} [\hat{n}_{m\sigma}(t), \hat{n}_{n\sigma'}] &= \frac{i}{N^2} \delta_{\sigma, \sigma'} \sum_{q, k, k'} \sin \left\{ (q-k)m \right. \\ &\quad \left. + (k-k')n - \frac{2J}{\hbar} [\cos(k) - \cos(q)]t \right\} \\ &\quad \times (\hat{c}_{q\sigma}^{\dagger} \hat{c}_{k'\sigma} + \text{H.c.}). \end{aligned} \quad (\text{A7})$$

Thus for zero temperature and half-filling, we obtain for the density response function

$$\begin{aligned} \chi_{mn}^R(t) &= \Theta(t) \frac{4}{\hbar N^2} \sum_{q, k} \sin \left\{ (q-k)(m-n) \right. \\ &\quad \left. - \frac{2J}{\hbar} [\cos(k) - \cos(q)]t \right\} \Theta[\cos(q)]. \end{aligned} \quad (\text{A8})$$

APPENDIX B: RANDOM PHASE APPROXIMATION FOR THE HUBBARD-MODEL

For the Hubbard-Hamiltonian in one dimension with N lattice sites and

$$\begin{aligned} \hat{K} &= \hat{H} - \mu \hat{N} \\ &= \sum_{k\sigma} \epsilon_k \hat{c}_{k\sigma}^{\dagger} \hat{c}_{k\sigma} + \frac{1}{2N} \sum_{\sigma} \sum_{k, k', q, q'} U_{qq'kk'} \hat{c}_{q\sigma}^{\dagger} \hat{c}_{q'\bar{\sigma}}^{\dagger} \hat{c}_{k'\bar{\sigma}} \hat{c}_{k\sigma}, \end{aligned} \quad (\text{B1})$$

where $\epsilon_k = -2J \cos(k) - \mu$, $U_{qq'kk'} = U \delta_{q+q', k+k'}$ and $\bar{\sigma} = -\sigma$, the density response function within the RPA takes the form

$$\chi_{\text{RPA}}^R(q, \omega) = \frac{2\Pi(q, \omega)}{1 - U\Pi(q, \omega)}, \quad (\text{B2})$$

where

$$\Pi(q, \omega) = \frac{1}{N} \sum_k \frac{n(\epsilon_k) - n(\epsilon_{k+q})}{\omega + \epsilon_k - \epsilon_{k+q} + i\eta}, \quad (\text{B3})$$

and $n(\epsilon_q) = \Theta[\cos(q)]$ for zero temperature and half-filling. The missing factor of 2 in Eq. (B3) and the extra factor of 2 in Eq. (B2) in comparison to the conventional form of these functions (compare [55]) are due to the unusual spin-indices in the Hamiltonian.

-
- [1] G. Giuliani and G. Vignale, *Quantum Theory of the Electron Liquid* (Cambridge University Press, Cambridge, 2005).
 - [2] A. Moreo, Magnetic susceptibility of the two-dimensional Hubbard model, *Phys. Rev. B* **48**, 3380 (1993).
 - [3] J. D. Lee, Spin fluctuations in the quarter-filled Hubbard ring: Significances to LiV_2O_4 , *Phys. Rev. B* **67**, 153108 (2003).
 - [4] A. Abendschein and F. F. Assaad, Temperature dependence of spectral functions for the one-dimensional Hubbard model: Comparison with experiments, *Phys. Rev. B* **73**, 165119 (2006).
 - [5] T. Dornheim, S. Groth, J. Vorberger, and M. Bonitz, *Ab initio* path integral Monte Carlo results for the dynamic

structure factor of correlated electrons: From the electron liquid to warm dense matter, *Phys. Rev. Lett.* **121**, 255001 (2018).

- [6] T. Dornheim, Z. A. Moldabekov, K. Ramakrishna, P. Tolias, A. Baczewski, D. Kraus, T. Preston, D. Chapman, M. Böhme, T. Doeppner, F. Graziani, M. Bonitz, A. Cangi, and J. Vorberger, Electronic density response of warm dense matter, *Phys. Plasmas* **30**, 032705 (2023).
- [7] M. Bonitz, T. Dornheim, Z. A. Moldabekov, S. Zhang, P. Hamann, H. Kählert, A. Filinov, K. Ramakrishna, and J. Vorberger, *Ab initio* simulation of warm dense matter, *Phys. Plasmas* **27**, 042710 (2020).

- [8] M. Bonitz, R. Binder, D. Scott, S. Koch, and D. Kremp, Theory of plasmons in quasi-one-dimensional degenerate plasmas, *Phys. Rev. E* **49**, 5535 (1994).
- [9] T. Dornheim, J. Vorberger, and M. Bonitz, Nonlinear electronic density response in warm dense matter, *Phys. Rev. Lett.* **125**, 085001 (2020).
- [10] T. Dornheim, M. Böhme, Z. A. Moldabekov, J. Vorberger, and M. Bonitz, Density response of the warm dense electron gas beyond linear response theory: Excitation of harmonics, *Phys. Rev. Res.* **3**, 033231 (2021).
- [11] X. Dong, X. Chen, and E. Gull, Dynamical charge susceptibility in the Hubbard model, *Phys. Rev. B* **100**, 235107 (2019).
- [12] S. Li and E. Gull, Magnetic and charge susceptibilities in the half-filled triangular lattice Hubbard model, *Phys. Rev. Res.* **2**, 013295 (2020).
- [13] R. G. Pereira, K. Penc, S. R. White, P. D. Sacramento, and J. M. P. Carmelo, Charge dynamics in half-filled Hubbard chains with finite on-site interaction, *Phys. Rev. B* **85**, 165132 (2012).
- [14] N.-H. Kwong and M. Bonitz, Real-time Kadanoff-Baym approach to plasma oscillations in a correlated electron gas, *Phys. Rev. Lett.* **84**, 1768 (2000).
- [15] L. Keldysh, Diagram technique for nonequilibrium processes, *Zh. Eksp. Teor. Fiz.* **47**, 1515 (1964) [*Sov. Phys. JETP* **20**, 1018 (1965)].
- [16] G. Stefanucci and R. van Leeuwen, *Nonequilibrium Many-Body Theory of Quantum Systems* (Cambridge University Press, Cambridge, 2013).
- [17] K. Balzer and M. Bonitz, *Nonequilibrium Green's Functions Approach to Inhomogeneous Systems* (Springer, Berlin, 2013).
- [18] N. Schlünzen, S. Hermanns, M. Bonitz, and C. Verdozzi, Dynamics of strongly correlated fermions: *Ab initio* results for two and three dimensions, *Phys. Rev. B* **93**, 035107 (2016).
- [19] N. Schlünzen, J.-P. Joost, and M. Bonitz, Achieving the scaling limit for nonequilibrium green functions simulations, *Phys. Rev. Lett.* **124**, 076601 (2020).
- [20] J.-P. Joost, N. Schlünzen, and M. Bonitz, G1-G2 scheme: Dramatic acceleration of nonequilibrium Green functions simulations within the Hartree-Fock generalized Kadanoff-Baym ansatz, *Phys. Rev. B* **101**, 245101 (2020).
- [21] J.-P. Joost, N. Schlünzen, H. Ohldag, M. Bonitz, F. Lackner, and I. Brezinova, The dynamically screened ladder approximation: Simultaneous treatment of strong electronic correlations and dynamical screening out of equilibrium, *Phys. Rev. B* **105**, 165155 (2022).
- [22] S. Donsa, F. Lackner, J. Burgdörfer, M. Bonitz, B. Kloss, A. Rubio, and I. Brezinov, Non-equilibrium correlation dynamics in the one-dimensional fermi-hubbard model: A testbed for the two-particle reduced density matrix theory, *Phys. Rev. Res.* **5**, 033022 (2023).
- [23] K. Balzer, N. Schlünzen, H. Ohldag, J.-P. Joost, and M. Bonitz, Accelerating nonequilibrium green function simulations with embedding self-energies, *Phys. Rev. B* **107**, 155141 (2023).
- [24] E. Schroedter, J.-P. Joost, and M. Bonitz, Quantum fluctuations approach to the nonequilibrium *GW*-approximation, *Condens. Matter Phys.* **25**, 23401 (2022).
- [25] Y. Klimontovich, On the method of second quantization in phase space, *JETP* **33**, 982 (1957).
- [26] Y. Klimontovich, Kinetic equations for classical nonideal plasmas, *JETP* **62**, 1770 (1972).
- [27] Y. L. Klimontovich, *Kinetic Theory of Nonideal Gases and Nonideal Plasmas* (Pergamon Press, Oxford, 1982).
- [28] S. Ayik, A stochastic mean-field approach for nuclear dynamics, *Phys. Lett. B* **658**, 174 (2008).
- [29] D. Lacroix, S. Hermanns, C. M. Hinz, and M. Bonitz, Ultrafast dynamics of finite Hubbard clusters: A stochastic mean-field approach, *Phys. Rev. B* **90**, 125112 (2014).
- [30] D. Lacroix and S. Ayik, Stochastic quantum dynamics beyond mean field, *Eur. Phys. J. A* **50**, 95 (2014).
- [31] V. Filinov, P. Thomas, I. Varga, T. Meier, M. Bonitz, V. Fortov, and S. W. Koch, Interacting electrons in a one-dimensional random array of scatterers: A quantum dynamics and Monte Carlo study, *Phys. Rev. B* **65**, 165124 (2002).
- [32] A. Polkovnikov, Phase space representation of quantum dynamics, *Ann. Phys.* **325**, 1790 (2010).
- [33] N. H. Kwong, M. Bonitz, R. Binder, and H. S. Köhler, Semiconductor Kadanoff-Baym equation results for optically excited electron-hole plasmas in quantum wells, *Phys. Status Solidi B* **206**, 197 (1998).
- [34] K. Balzer, N. Schlünzen, and M. Bonitz, Stopping dynamics of ions passing through correlated honeycomb clusters, *Phys. Rev. B* **94**, 245118 (2016).
- [35] K. Balzer, M. R. Rasmussen, N. Schlünzen, J.-P. Joost, and M. Bonitz, Doublon formation by ions impacting a strongly correlated finite lattice system, *Phys. Rev. Lett.* **121**, 267602 (2018).
- [36] A. Niggas, J. Schwestka, K. Balzer, D. Weichselbaum, N. Schlünzen, R. Heller, S. Creutzburg, H. Inani, M. Tripathi, C. Speckmann, N. McEvoy, T. Susi, J. Kotakoski, Z. Gan, A. George, A. Turchanin, M. Bonitz, F. Aumayr, and R. A. Wilhelm, Ion-induced surface charge dynamics in freestanding monolayers of graphene and MoS₂ probed by the emission of electrons, *Phys. Rev. Lett.* **129**, 086802 (2022).
- [37] D. Kremp, M. Schlanges, and W. Kraeft, *Quantum Statistics of Nonideal Plasmas* (Springer, Berlin, 2005).
- [38] For two single-particle quantities A and B , we define the commutator as $[A, B]_{ij} := \sum_k \{A_{ik}B_{kj} - B_{ik}A_{kj}\}$.
- [39] M. Bonitz, *Quantum Kinetic Theory*, 2nd ed., Teubner-Texte zur Physik (Springer, Cham, 2016).
- [40] P. Lipavský, V. Špička, and B. Velický, Generalized Kadanoff-Baym ansatz for deriving quantum transport equations, *Phys. Rev. B* **34**, 6933 (1986).
- [41] M. Bonitz, D. Kremp, D. C. Scott, R. Binder, W. D. Kraeft, and H. S. Köhler, Numerical analysis of non-Markovian effects in charge-carrier scattering: one-time versus two-time kinetic equations, *J. Phys.: Condens. Matter* **8**, 6057 (1996).
- [42] M. Bonitz, Correlation time approximation in non-Markovian kinetics, *Phys. Lett. A* **221**, 85 (1996).
- [43] E. Schroedter and M. Bonitz, Two-time Quantum fluctuations approach and its relation to the Bethe-Salpeter equation (unpublished).
- [44] Note that the polarization approximation, the BSE, and RPA may differ in their level of self-consistency at which the equations are treated. For example, often within the RPA, the single-particle Green functions that enter the BSE for the XC function, cf. Eq. (36), are calculated at the level of the self-energy that forms the basis for the irreducible vertex, i.e., the Hartree self-energy [56]. Within the *GW* approximation, the

- same BSE for L is used, but the KBE for the single-particle Green functions includes screening effects described via the XC function. Moreover, in the HF-GKBA, the self-consistency of the equations is treated at an intermediate level, as the reconstruction of the time-off-diagonal Green function is done using Hartree-Fock propagators, which implicitly include screening effects. Within the validity of the considered approximations, i.e., in the weak-coupling limit, however, the different treatment of self-consistency of these approaches is negligible. Thus, these approaches can be considered equivalent within their applicability limits.
- [45] S. Hermanns, N. Schlünzen, and M. Bonitz, Hubbard nanoclusters far from equilibrium, *Phys. Rev. B* **90**, 125111 (2014).
 - [46] N. Schlünzen, S. Hermanns, M. Scharnke, and M. Bonitz, Ultrafast dynamics of strongly correlated fermions – Nonequilibrium Green functions and selfenergy approximations, *J. Phys.: Condens. Matter* **32**, 103001 (2020).
 - [47] I. Ulgen, B. Yilmaz, and D. Lacroix, Impact of initial fluctuations on the dissipative dynamics of interacting fermi systems: A model case study, *Phys. Rev. C* **100**, 054603 (2019).
 - [48] An extension to systems with finite temperature and bosonic systems is straightforward.
 - [49] This approach can be easily generalized to arbitrary spin configurations.
 - [50] We assume equidistant sites throughout our further considerations.
 - [51] K. Balzer, S. Hermanns, and M. Bonitz, Electronic double excitations in quantum wells: Solving the two-time Kadanoff-Baym equations, *Europhys. Lett.* **98**, 67002 (2012).
 - [52] F. H. L. Essler, H. Frahm, F. Göhmann, A. Klümper, and V. E. Korepin, *The One-Dimensional Hubbard Model* (Cambridge University Press, Cambridge, 2005).
 - [53] N. Schlünzen, J.-P. Joost, F. Heidrich-Meisner, and M. Bonitz, Nonequilibrium dynamics in the one-dimensional Fermi-Hubbard model: Comparison of the nonequilibrium Green-functions approach and the density matrix renormalization group method, *Phys. Rev. B* **95**, 165139 (2017).
 - [54] N. Schlünzen and M. Bonitz, Nonequilibrium green functions approach to strongly correlated Fermions in lattice systems, *Contrib. Plasma Phys.* **56**, 5 (2016).
 - [55] A. Altland and B. D. Simons, *Condensed Matter Field Theory*, 2nd ed. (Cambridge University Press, Cambridge, 2010).
 - [56] G. Baym and L. P. Kadanoff, Conservation laws and correlation functions, *Phys. Rev.* **124**, 287 (1961).